# MXenes—A New Class of Two-Dimensional Materials

Subjects: Materials Science, Characterization & Testing

Contributor: Kateryna Smyrnova

A new class of two-dimensional nanomaterials, MXenes, which are carbides/nitrides/carbonitrides of transition and refractory metals, has been critically analyzed. Since the synthesis of the first family member in 2011 by Yury Gogotsi and colleagues, MXenes have quickly become attractive for a variety of research fields due to their exceptional properties. Despite the fact that this new family of 2D materials was discovered only about ten years ago, the number of scientific publications related to MXene almost doubles every year. Thus, in 2021 alone, more than 2000 papers are expected to be published, which indicates the relevance and prospects of MXenes.

MXene two-dimensional materials carbides properties selective etching

## 1. Introduction

Studies of nanolayer two-dimensional materials date back to the 1950s [1][2]. Due to the discovery of graphene, it attracted the attention of many researchers for their methods of preparation, properties, and possible applications. Graphene has already demonstrated outstanding characteristics in terms of electrical conductivity, optical transparency, mechanical strength, and thermal conductivity [3][4]. Deep interest in graphene research facilitated the start of new two-dimensional solid materials, such as silicene, phosphorene, h-BN, and $MoS_2$ [5][6][7][8]. These two-dimensional layered materials exhibit unusual electrical properties due to their unique characteristics, e.g., it is possible to place various ions or molecules between their layers [9].

In 2011, researchers from Drexel University discovered a new class of inorganic compounds with a two-dimensional structure, which aroused great interest among scientists from all over the world [10]. These unusual 2D materials were called MXenes. The family of MXenes consists of carbides, nitrides, or carbonitrides of transition metals. They are two-dimensional nanolayers with the thickness of several atoms and a planar size in the order of several micrometers [9][11][12][13]. MXene materials have a wide range of unique properties that make them attractive and suitable for a variety of applications [14][15][16]. For example, they have a large specific surface area and high mechanical, electronic, and physicochemical properties, as well as excellent biocompatibility [17][18].

To synthesize MXenes, MAX phases are used as the main precursor material. Their generalized formula is $M_{n+1}AX_n$, where M is an early transition metal, A is any element from IIIA or IVA (13–14) groups, X is carbon or nitrogen, but the combinations with the formation of carbonitride are also possible, and n = 1 − 4 [19]. Thus, the preceding $M_{n+1}AX_n$ phases have a hexagonal structure ($P6_3/mmc$ symmetry). In their simplest units, two constituent structural entities can be distinguished: octahedral "$M_6X$" units with common edges, identical to the

cubic face-centered lattice of NaCl of the type of binary nitrides or carbides, as well as the layers of the A element located between them. In this case, the X atoms are located in the space of octahedral interstices. It should be noted that the chemical bonds between the transition metal M and the X atom have a mixed character (metallic, ionic, and covalent components are present), while the M–A bonds are represented only by the metallic component. Therefore, the metal bond is weaker than the covalent one, and by choosing a suitable reagent for etching, it is possible to break the M–A bond and remove the elements of the A layer [20]. Consequently, selective etching of element A (for example, Al, Si, Ga, In, and S) leads to the formation of layered $M_{n+1}X_n$ with an "accordion-like" structure. Sometimes the formula $M_{n+1}X_nT_x$ is used, where T is added to denote surface functional groups, for example, O, F, OH, $H_2O$, and/or Cl [21]. The MXene layers obtained by etching the A element form various surface functional groups depending on the substance with which they react. Such reactions make it possible to control their physicochemical properties. For example, reacting with hydrofluoric acid (HF) and $H_2O$, $Ti_3C_2$ acquires an F- and O/OH-terminated surface [22].

## 2. Methods to Synthesize MXenes

After successful synthesis of the first layered $Ti_3C_2T_x$ using hydrofluoric acid, several other methods were developed and implemented to obtain various MXenes with new compositions. To date, there are two different strategies for obtaining MXenes using the “top-down” and “bottom-up” approaches (**Figure 1**). The main difference between these strategies is that the top-down synthesis method involves the separation of bulk materials, for example MAX phases, into several layers, while the bottom-up method uses the MXene deposition technology, forming the material from the bottom to the top. It should be noted that, depending on the synthesis method, the properties of the MXenes may differ. In addition, the characteristics of two-dimensional transition metal carbides/nitrides/carbonitrides depend on the starting material that is used to obtain them as well as various surface modification technologies. Therefore, a closer look is required to overview the main steps in the process of MXene synthesis and to identify the advantages and disadvantages of various strategies.

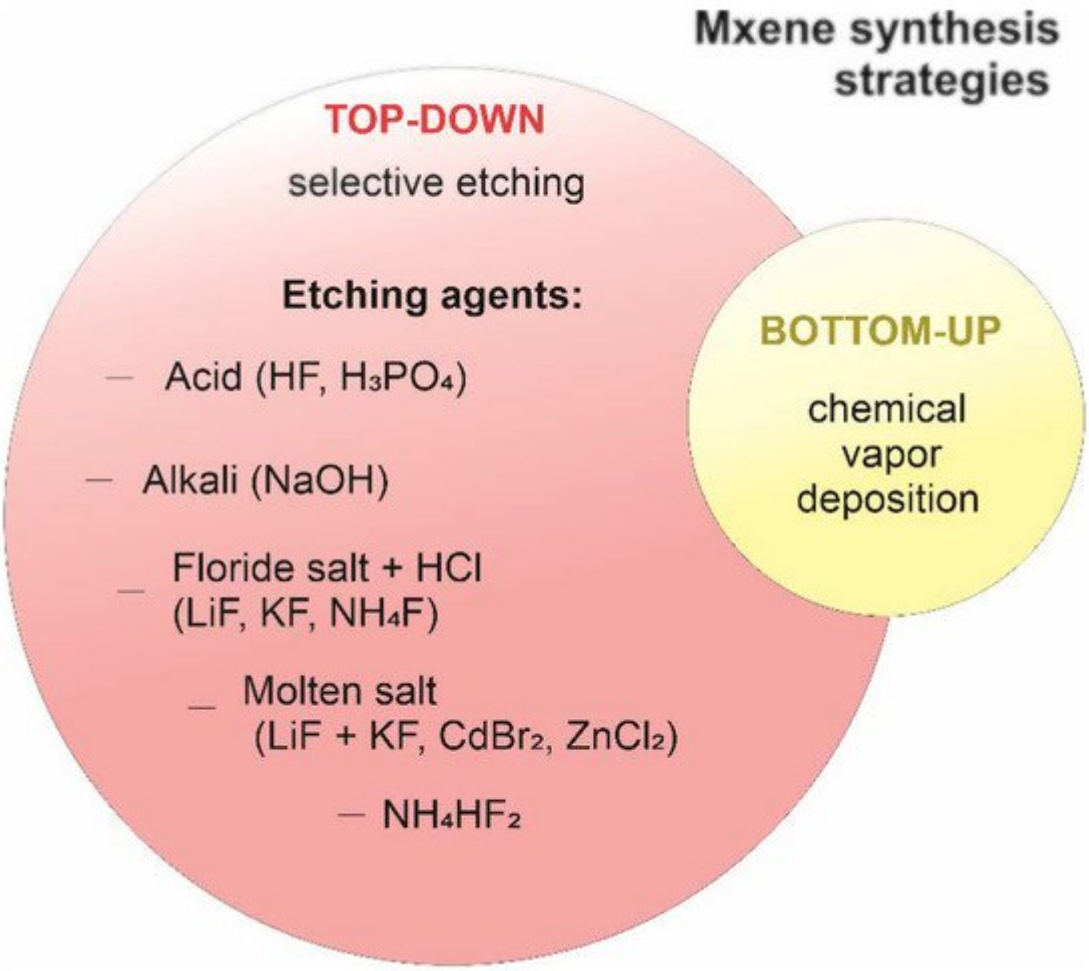


**Figure 1.** Methods for obtaining MXenes and examples of reagents used for selective etching of MAX phases or other precursor materials.

## 3. MXene Applications

Having received the first representative of the new family of two-dimensional materials with unique properties, MXenes have become one of the most popular areas of modern science [23]. Their active study led to the rapid discovery of new transition metal carbides/nitrides/carbonitrides with various chemical compositions, structures, and characteristics. It has been found that, due to the wide range of properties inherent to MXenes, they can be successfully used for various applications. For example, the outstanding electrical and optical properties of these two-dimensional materials may be of interest to design sensors [24]. They also demonstrated strong absorption in the near-infrared region, low cytotoxicity, high biocompatibility, and even some selectivity towards cancer cells, making them attractive candidates for bioimaging, photothermal therapy, theranostics, and drug delivery in the human body [25]. The development of electrical power systems causes a need for new dielectrics, which must exhibit low dielectric loss and high dielectric constant to be suitable for electrostatic film capacitors with high energy density, flexibility, and high breakdown strength. It was found that incorporation of MXene nanosheets to polymer allows achieving the optimal combination of high dielectric constant and low dielectric loss [26]. For instance, poly(vinylidene fluoride) (PVDF)-based percolative composites with 2D $Ti_3C_2T_x$ nanosheets as fillers reached a

dielectric constant as high as $10^5$ near the percolation limit (15.3 wt.% MXene) [27]. Moreover, the dielectric loss of the MXene/P(VDF-TrFE-CFE) composite increased from 0.06 to 0.35 (5-fold), but the dielectric constant increased by 25 times within 0–10 wt.% MXene composition range. The origin of the substantial permittivity enhancement is primarily due to the microscopic dipoles formed by the accumulation of charges at the interfaces between the MXene fillers and the polymer matrix. Compared with other fillers (hydrothermally reduced graphene oxide, copper phthalocyanine, functionalized graphene nanosheets), MXenes provided the best dielectric constant/loss factor trade-off. The other example of such composite is multilayered $Ti_3C_2T_x$/PVDF films fabricated by three steps: spin coating, spray coating, and hot-press methods [26]. This structure consisted of overlapped layers of MXene and PVDF placed on each other to provide enhanced interfacial interactions due to $Ti_3C_2T_x$ and good charge carrier insulation through the ferroelectric PVDF layer. The dielectric constant of the multilayer 4MXene/5PVDF (four layers of $Ti_3C_2T_x$ and five layers of PVDF) measured at 1 kHz was about 41, higher than that of pure PVDF (10.5). An increase was caused by enhanced Maxwell–Wagner–Sillars (MWS) interfacial polarization due to the difference in dielectric performances of $Ti_3C_2T_x$ and PVDF. The dielectric loss at 1 MHz was suppressed below 0.2. Additionally, MXene/PVDF films had low conductivity of $<10^9$ S $m^{-1}$ at 1 kHz. The frequency-dependent alternating current (AC) conductivity suggested an insulating behavior of the composite films. It also demonstrated a superior dielectric constant to loss factor ratio of about 1464.3. Therefore, composite MXene-based films are promising broadband dielectric material for high-frequency capacitors. Another example of the use of MXene phases as reinforcement in ceramic composites is $Ti_3C_2T_x/Al_2O_3$, which at 2 wt.% of $Ti_3C_2T_x$ showed a 300%, ~150%, and ~300% improvement of the fracture toughness, bending strength, and hardness, respectively [28]. The ZnO-$Ti_3C_2$ composite produced by the cold sintering process improved the electrical conductivity of the oxide matrix by 1–2 orders of magnitude and showed a 150% increase in hardness and elastic modulus [29]. The enhancement of mechanical properties of silicon carbide modified with $Ti_3C_2T_x$ was also reported by Petrus et al. [30]. The $Ti_3C_2T_x$ MXene composite films with segregated polystyrene inclusions studied by Iqbal et al. [31] showed superior electromagnetic interference efficiency, making them a promising shielding material with tunable electromagnetic wave absorption properties. Furthermore, the combination of MXenes as nanofillers with polymers allows preparing the flame retardant nanocomposites [32]. The unique layered structure and versatile interface chemistry of 2D MXenes make it possible to improve polymer properties [33]. For instance, the addition of 2.0 wt.% $Ti_3C_2Tx$ into unsaturated polyester resin (UPR) resulted in the formation of nanocomposite with an enhanced fire safety property: the peak heat release rate, the total smoke production, and carbon monoxide production were reduced by 29.56%, 25.26%, and 31.58%, respectively [34]. Yu et al. manipulated the surface of $Ti_3C_2T_x$ with 3-aminopropylheptaisobutyl-polyhedral oligomeric silsesquioxane (AP-POSS) through electrostatic interactions and incorporated the POSS-$Ti_3C_2T_x$ into polystyrene (PS). The resultunt PS nanocomposites exhibited 39.1%, 54.4%, and 35.6% reductions in the peak heat release rate, the CO production rate, and the $CO_2$ production rate, respectively [35]. Thus, MXenes are popular materials with many possible applications in various industries. Some of them are schematically shown in **Figure 2**.

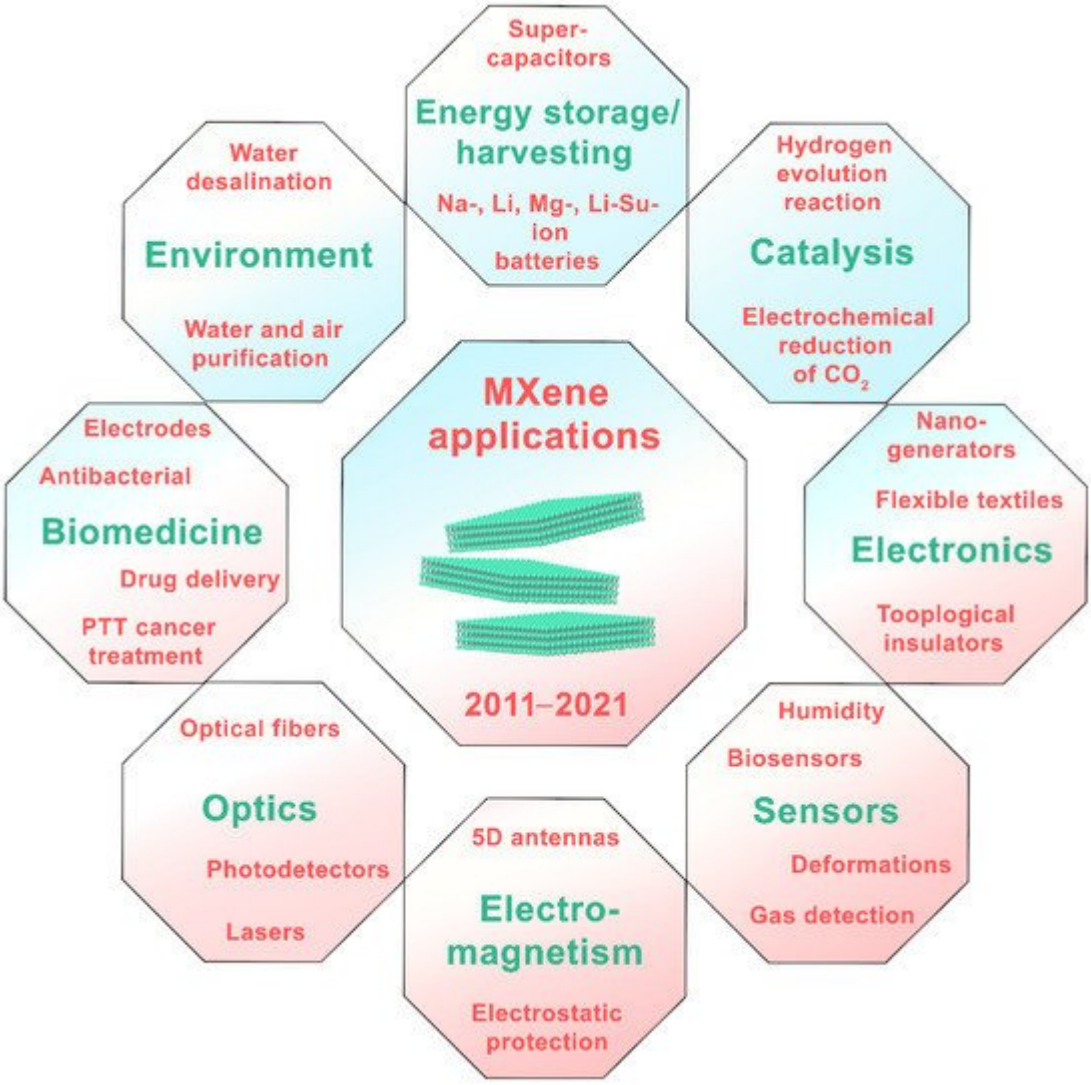


**Figure 2.** Possible applications of two-dimensional MXene in various industries.

### 3.1. Biomedicine

Two-dimensional MXenes are being actively investigated for their potential medical applications. For example, the large surface area of their ultrafine planar structure provides numerous anchorage sites for drug molecules. MXene nanosheets inherently possess excellent photothermal converting properties that can be further developed as photothermal nanoagents for cancer hyperthermia when exposed to external near-infrared (NIR) laser irradiation. In recent years, MXenes have been applied as agents for photo-thermal therapy (PTT), as a bioimaging technology, for drug delivery, and as an antibacterial substance and electroconductive base in biomaterial applications. In the current review, we cover two of the most popular applications of MXenes: a cancer treatment strategy and an antibacterial/antiviral therapy.

#### 3.1.1. Photo-Thermal Therapy

Photo-thermal therapy (PTT) emerge as promising non-invasive and light-triggered anti-cancer approaches [36]. PTT generates heat by transforming near-infrared (NIR) light into thermal energy in a minimally invasive manner,

which is regarded as the potential treatment substitution for conventional clinical cancer therapeutic modalities [37]. Gold nanoparticles, graphene, transition metal dichalcogenides, black phosphorus, and some organic nanosystems are promising agents for PTT [38]. MXenes are the wide-spectrum photothermal-conversion agents that can be activated in both NIR-I (750–1000 nm) and NIR-II (1000–1350 nm) biowindows that allow maximal penetration to the living tissues [39]. NIR-II demonstrates higher maximum permissible exposure and penetration depth than the NIR-I [40], but their application depends on the extinction coefficient on MXenes.

$Ti_3C_2$ was the first MXene applied for PTT both in vitro and in vivo [41] due to its high extinction coefficient and low toxicity. $Ti_3C_2$ exhibits a high extinction coefficient of 25.2 L $g^{-1}$ $cm^{-1}$, which is remarkably higher than that of traditional Au nanorods (13.9 L $g^{-1}$ $cm^{-1}$) [42], indicating a favorable NIR laser-absorption property of $Ti_3C_2$ nanosheets. Lin at all. first described the possible application of $Ti_3C_2$ for in vitro and in vivo photothermal ablation. They demonstrated high biocompatibility of a $Ti_3C_2$–soybean phospholipid (SP) complex in concentration up to 400 μg/mL using 4T1 cancer cell line. 4T41 cells were incubated with $Ti_3C_2$–SP nanosheets at varying concentrations (0, 6, 12, 25, 50, and 100 μg/mL) for 4 h and then exposed to the 808 nm laser at a power density of 1.0 W $cm^{-2}$. They proved the photothermal ablation effect of $Ti_3C_2$–SP that strongly depends on MXene concentration [41]. The in vivo investigation demonstrated 1.73% $Ti_3C_2$–SP accumulation in tumors within 24 h after intravenous injection on nude mice with no adverse effect on living organs. The tumor on the $Ti_3C_2$–SP–NIR group was completely eliminated after 16 days of observation. In 2017, Liu et al. established $Ti_3C_2$ multifunctional nanoplatforms via layer-by-layer surface modification with doxorubicin (DOX) and hyaluronic acid (HA) [43]. The $Ti_3C_2$–DOX complex demonstrates potential application for combine the PTT-chemotherapy approach with high biocompatibility, tumor-specific accumulation, and stimuli-responsive drug release behavior. They demonstrate no toxicity for both unmodified $Ti_3C_2$ nanosheets and $Ti_3C_2$–DOX complex in concentration up to 200 μg/mL. 808 nm laser irradiation (0.8 W $cm^{-2}$) demonstrated HCT-116 cells death both from PTT effect and DOX release because of the disruption of electrostatic interaction in the $Ti_3C_2$–DOX system. Xiaoxia Han in 2018 reported a similar PTT effect of DOX–$Ti_3C_2$–SP complexes against 4T1 timer cells in vitro as well as high effectiveness on 4T1 tumor-bearing nude mice [44]. A NIR 808 nm laser with 1.5 W $cm^{-2}$ power after 10 min irradiation leads to tumor reduction in the DOX–$Ti_3C_2$–SP group. The authors demonstrated that $Ti_3C_2$ MXene had a high drug-loading capability (211.8%) and exhibited both pH-responsive and NIR laser-triggered on-demand drug release. Later, some authors showed different $Ti_3C_2$ modification and high PTT effectiveness in NIR-I region of MXene-cellulose-DOX complexes [45], Plasmonic MXene-based nanocomposites (Au/MXene and Au/$Fe_3O_4$/MXene) [46], $Ti_3C_2$–cobalt nanowire–DOX construction [47], $Ti_3C_2$–metforminpolysaccharide composites [48] and $Ti_3C_2$–superparamagnetic iron oxide nanoparticles [49]. All these researches demonstrated the possible applications of $Ti_3C_2$ MXenes for PTT and as a promising platform for combined photo-dynamic and chemotherapy.

In contrast with $Ti_3C_2$, $Nb_2C$ MXenes exhibit effectiveness in both NIR-I and NIR-II regions. In 2017, Lin et al. described a highly efficient $Nb_2C$–PVP nanosheet in vivo photothermal ablation of mouse tumor xenografts in both NIR-I and NIR-II windows. They used 4T1 cells as cancer model and 5 min of 808 nm and 1064 nm laser irradiation after MXene-cell co-incubation. $Nb_2C$-PVP intravenous injection on the 4T1 tumor-bearing mice with next NIR-I and NIR-II irradiation within 10 min led to significant tumor size reduction compared to control groups [50]. A year later, Han et al. demonstrated the synthesis of $Nb_2C$–arginine–glycine–aspartic pentapeptide c(RGDyC)

and its effectiveness in NIR-II PTT against U87 cancer cell line and corresponding tumor xenograft with 92.7% inhibition efficiency [39]. In 2019, Xiang and co-authors engineered a free radical nanogenerator via direct growth of mesoporous silica layer onto the surface of two-dimensional $Nb_2C$ MXene nanosheets toward multifunctionality, where the mesopore provided the reservoirs for initiators, and the MXene core acted as the photonic thermal trigger at the NIR-II region. The 1064 nm laser irradiation induced the fast release and quick decomposition of the encapsulated initiators (AIPH) to produce free radicals that provided additional effects to 4T1 cancer cells [51].

Some research demonstrated the possible application of $V_2C$ and $Ta_4C_3$ MXene for PTT cancer treatment. Zada et al. demonstrated high photothermal conversion efficiency of $V_2C$ MXenes with effectiveness against MCF-7 cancer cell line and MCF-7 tumor-bearing mice in the NIR-I region (808 nm). Additionally, they proved that significant photoacoustic (PA) and magnetic resonance (MR) signals were observed even at low concentrations in vitro and in vivo that open perspectives for bio-imaging [52]. Zhuang Liu in 2018 demonstrated the possible application of $Ta_4C_3$ MXenes for theranostics. Functionalized superparamagnetic iron-oxide MXene composite ($Ta_4C_3$-IONP-SPs) exhibited high performance for contrast-enhanced CT imaging and significant effectiveness against 4T1 breast cancer cells after irradiation in NIR-I (808 nm) regions.

Based on available data, there are two possible mechanisms of direct MXene anticancer PTT. Cell membrane adsorption of MXenes and their penetration inside the cancer cell lead to direct cell death after photothermal conversion of NIR light (**Figure 3**a). The heating of intercellular media leads to mediated cell death via the initiation of apoptosis (**Figure 3**b). Chemotherapeutic drugs and nanoparticles loaded to MXene can provide additional effects and secure complete anticancer therapy.

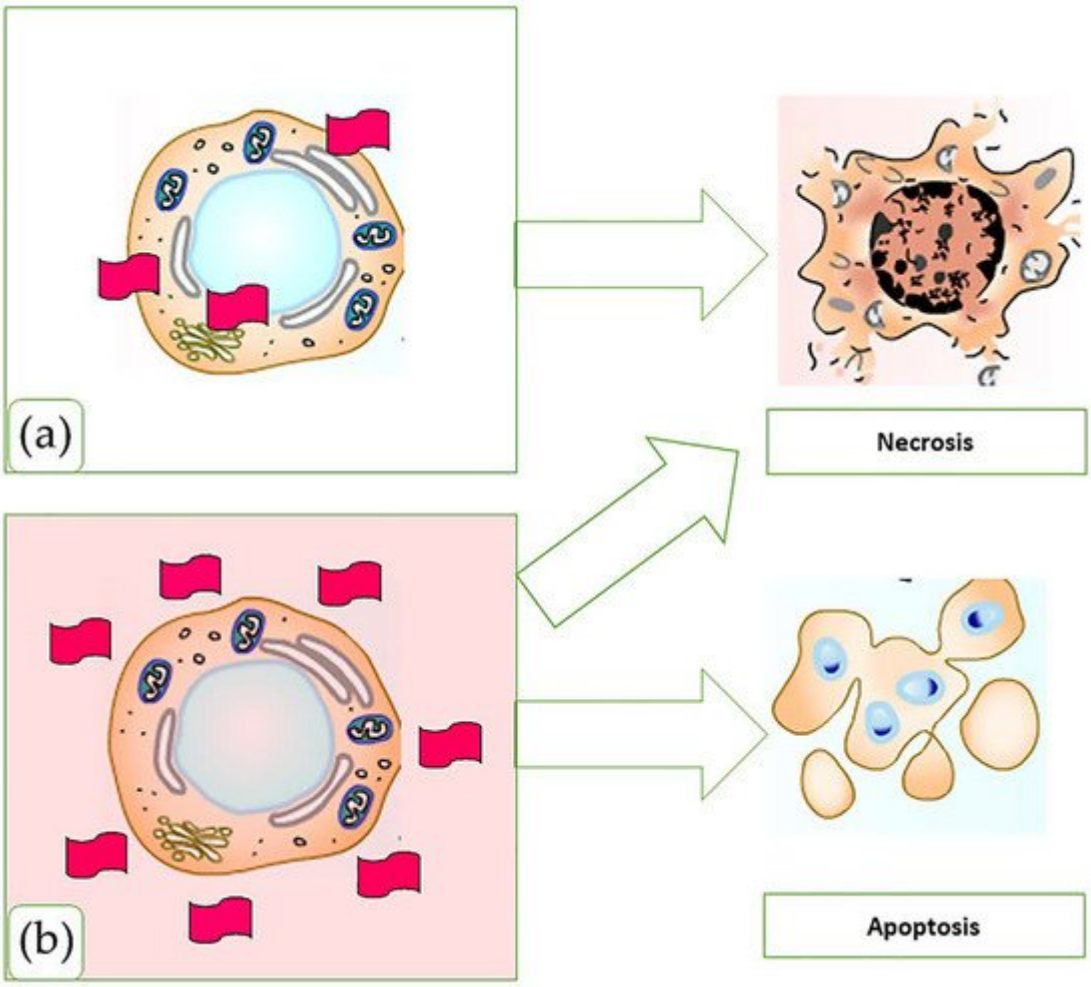


**Figure 3.** Proposed mechanisms of anticancer effects of MXenes (figure description provided in the main text).

To summarize, a variety of MXenes demonstrated the ability for PTT as is and as a part of complexes, including chemotherapy agents, bioactive substances, and magnetic nanoparticles. Most research proved low toxicity and high effectiveness against different cancer cell lines both during in vitro and in vivo experiments. NIR-I and NIR-II laser irradiation could be applied for PTT with respect to MXene nature, but most research used an 808 nm wavelength. Considering the high loading capacity of MXene and the active surface, chemotherapeutic and ROS agents could be used for combined chemotherapy and PDD approaches. Loading MXenes with specific anti-cancer antibodies can provide a new approach in target cancer PTT with minimal side effects and MXene accumulation in tissues. Despite a large amount of research, the biological effect of MXenes is still under question, including full metabolic fate, long-term side effects, and influence on immune cells.

### 3.1.2. Antibacterial Activity

The first report about the antibacterial activity of MXene was presented by Y. Gogotsi and co-authors in 2016 [53]. They utilized *Escherichia coli* (E. coli) and *Bacillus subtilis* (B. subtilis) strains to assess the antibacterial activity of $Ti_3C_2T_x$ MXenes. 100 µg/mL $Ti_3C_2T_x$ within 4 h of exposure demonstrated more than 98% effectiveness against both Gram-negative and Gram-positive bacteria. Authors clearly observed dose-depending bacteria effectiveness for both strains with more substantial influence to Gram-positive ones that could relate with more negatively

charged surface of Gr(+) bacteria wall. Using SEM, the authors showed severe membrane disruption and cytoplasm leakage after bacteria co-cultivation with 100 µg/mL of $Ti_3C_2T_x$. HRTEM demonstrated the presence of the highly crystalline $Ti_3C_2T_x$ layers that could directly affect the cell wall. Additionally, the authors hypothesized that, due to the high conductivity of MXenes, a conductive bridge over the insulating lipid bilayer could form that mediated electron transfer from bacterial intracellular components to the external environment and caused the bacteria cell death. Later, the same group developed a micrometer-thick titanium carbide ($Ti_3C_2T_x$) MXene membranes prepared by filtration on polyvinylidene fluoride (PVDF) support for applications in water/wastewater treatment. The membrane provided 73% effectiveness against B. subtilis and 67% against E. coli [54]. It is remarkable that the aged $Ti_3C_2T_x$ membrane increased effectiveness up to 99% against both microbial strains.

Mayerberger et al. produced an electrospun membrane with encapsulated delaminated $Ti_3C_2T_z$ (MXene) flakes within chitosan nanofibers for passive antibacterial wound dressing applications. 0.75 wt.% $Ti_3C_2T_z$- loaded nanofibers provided 95% effectiveness against Escherichia coli and Staphylococcus aureus with no cell toxicity [55].

Jastrzębska et al. studied the antibacterial activity of $Ti_2C$ and $Ti_3C_2$ against E. Coli using the classical culture method. They did not find any bacteria inhibition with $Ti_2C$ flakes and only a small inhibition zone (up to 1.5 mm) around the $Ti_3C_2$ MXenes [56]. From our experience, the contact inhibition after direct MXene-cell membrane interaction that was proved in [57] should be noted. Later, using a broth microdilution assay, Shamsabadi et al. proved that direct contact between MXene and cell membrane plays a crucial role in the antibacterial mechanism of action. They demonstrated that the sharp age of small size MXene (lateral size less than 0.57 µm) leads to bacterial cell wall damage and DNA release from the cytosol [58]. Another group stabilized $Ti_3C_2$ MXene surface using poly-L-lysine (PLL) that changed the negatively charged cell surface to a positive value and stabilized colloidal solution of MXenes. These changes provided an additional antibacterial effect of MXene solution towards E. Coli compared to non-modified $Ti_3C_2$ [59]. Another approach used to enhance MXene antibacterial properties was implemented by Zheng et al. through conjugating ultra-small gold nanoclusters (AuNCs) on $Ti_3C_2$ nanosheets. They proved an synergic antimicrobial mechanism via mechanical damage of the cell membrane by MXenes and oxidizing of bacterial membrane lipid and bacterial DNA for violent fragmentation via reactive oxygen species generated by AuNCs [60]. Pandey et al. proposed MXene modification with Ag nanoparticles (Ag@MXene) as an alternative for water purification membranes. Their 21% Ag@MXene composite membrane exhibited 99% effectiveness against the E. Coli strain compared to the 60% effectiveness of a pure MXene-loaded membrane. This synergetic effect should be used for water purification and biomedical applications [61].

Another strategy for MXene exploitation as antibacterial agents is applying NIR light to provide photo-thermal ablation. Wu et al. demonstrated high effectiveness for $Ti_3C_2$ MXene combined with 808 nm light (20 min irradiation) against 15 bacterial spices [62]. Remarkable that this method demonstrates effectiveness against methicillin-resistant *Staphylococcus aureus* (MRSA) and vancomycin-resistant *Enterococci* (VRE) as well as against MRSA biofilms.

The latest research demonstrates the antiviral and immunomodulatory potential of MXenes [63]. Unal et al. tested four MXenes, $Ti_3C_2T_x$, $Ta_4C_3T_x$, $Mo_2Ti_2C_3T_x$, and $Nb_4C_3T_x$, as antiviral agents against four viral clades. They found

that $Ti_3C_2T_x$ reduced infection in SARS-CoV-2/clade GR-infected Vero E6 cells. $Mo_2Ti_2C_3T_x$ also exhibited antiviral activity compared to the $Ta_4C_3T_x$ and $Nb_4C_3T_x$ ones. Additionally, they tested MXene interaction with 17 subpopulations of human primary immune cells and concluded that all tested MXenes had excellent bio and immune compatibility with the ability to reduce the release of pro-inflammatory cytokines.

Based on the abovementioned data, we summarized the possible antibacterial mechanisms of MXenes in **Figure 4**. Nevertheless, in conclusion, it should be noted that antibacterial activity was proved only for $Ti_3C_2$ MXenes against a few bacterial spices. A more detailed study of the antibacterial spectrum is needed to ensure precise bactericidal mechanisms. Detailed investigation of toxicity/bactericidal balance must also be performed using different MXene compositions. The optimal parameters, including size, composition, and additives, need to be clarified to open clinical application.

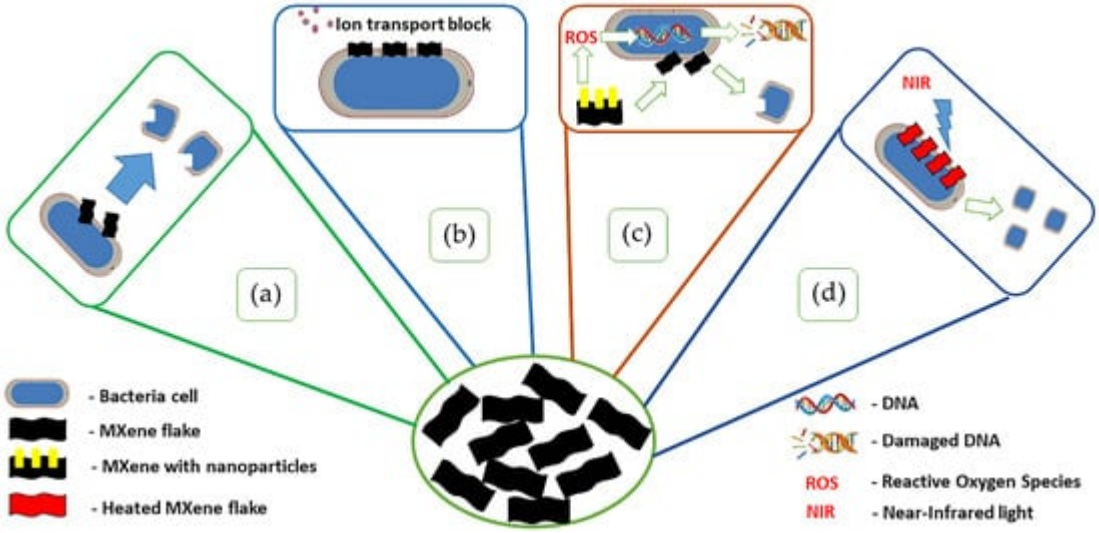


**Figure 4.** The scheme of proposed mechanisms of MXene antibacterial activity. (**a**)—a direct invasion of sharp MXene to bacteria wall with cell membrane disintegration; (**b**)—formation of the conductive bridge over the insulating lipid bilayer and ion transport block; (**c**)—MXene-AuNCs provide direct MXene invasion to bacteria cells with formation of ROS by AuNCs and DNA damage; (**d**)—photo-thermal ablation of bacteria after NIR light irradiation of MXenes.

## 3.2. Ecological/Environmental Applications

With the rapid growth of the world population and the rise of agriculture and industrial production, a shortage of drinking water is predicted [64]. Therefore, the development of new methods for obtaining clean, fresh water is one of humankind's most important global problems [65]. To improve water quality, it is necessary to remove harmful impurities that can negatively affect human health and the environment. For example, some of the most common pollutants are heavy metal ions, toxic gases, dyes, hormones, and organic solvents [64]. Among all water pollutants, heavy metal ions (Pb (II), Cr (VI), Hg (II), and U (VI)) are in first place in terms of toxicity to the human body. It is also important to purify water from various organic dyes that are difficult to biodegrade due to their stable molecular

structure [66]. Recently, photothermal conversion, membrane separation, and adsorption have become the most popular water purification methods [67][68][69].

### 3.2.1. Photothermal Conversion

Studies show that natural renewable energy sources such as solar radiation can be effectively used for the purification, distillation, and desalination of seawater [70]. For such purposes, solar steam generators based on the principle of photothermal conversion have demonstrated their effectiveness. In the classical solar steam generators, solar energy is absorbed by the receiver and is then used to heat up the main fluid due to thermal conductivity and thermal convection [64][71]. The coefficient of performance (COP) of such systems is less than 50% since most of the absorbed solar thermal energy is used to heat the main fluid. For efficient water evaporation due to light absorption and reduction of heat losses in the system, the evaporator must have high hydrophilicity and photothermal conversion, excellent light absorption characteristics, and a porous structure to ensure sufficient water supply to the absorbers [72]. In addition, photothermal materials should not sink the water since placement directly at the water–air interface reduces heat loss to bulk water. Recent studies have shown that MXene exhibits high efficiency in absorbing solar energy and has great potential for solar steam generator applications [73].

For example, in 2017, the most popular representative of the MXene family, $Ti_3C_2$, was studied as a solar photothermal material [73]. For its synthesis, the $Ti_3AlC_2$ MAX phase was used, which was treated with an aqueous solution of HF for selective etching of aluminum, followed by immersion in DMSO and sonication. After that, the aqueous suspension of MXenes was filtered through a hydrophilic membrane of polyvinylidene fluoride (PVDF) 0.22 μm thick. Thus, a thin layer of stacked MXene sheets was formed on the surface of the PVDF substrate. To test the characteristics of photothermal water evaporation, the MXene–PVDF photothermal membrane was modified by adding functional groups using a solution of polydimethylsiloxane (PDMS) in hexane. $Ti_3C_2$ demonstrated close to 100% light to heat conversion and excellent light absorption. In this case, the wavelength of the laser source, 473 or 785 nm, did not adversely affect the efficiency of titanium carbide in any way, which indicates the ideal characteristics of photothermal conversion. In addition, a thin MXene-PVDF membrane with a thermal barrier provided a photothermal evaporation efficiency of about 84%. The disadvantage of such a membrane was that it was wetted in water, although, after modification with PDMS, it could float on the surface of water on its own. The non-wetting surface naturally repels water and prevents it from entering the membrane during desalination with the help of solar radiation [74]. Such high characteristics of $Ti_3C_2$ suggest that MXene-based membranes can provide effective water purification from contamination and environmentally friendly long-term operation [75].

Later, in 2018, a self-floating solar steam generator for water desalination based on a hydrophobic membrane with $Ti_3C_2$ was presented [74]. Two-dimensional titanium carbide nanosheets were synthesized by etching the $Ti_3AlC_2$ MAX phase with an HCl/LiF solution. The MXene membrane was prepared by filtering delaminated $Ti_3C_2$ nanosheets modified with a hydrolysis solution of perfluorodecyltrimethoxysilane (PFDTMS) (0.5 vol.% acetic acid, 2.0 vol.% PFDTMS, and 97.5 vol.% isopropanol) onto a mixed ester membrane cellulose with a pore size of 0.22 μm. The solar steam generator device consisted of three components: membrane with $Ti_3C_2$ on filter

membrane (solar energy absorber, vapor generator, and salt blocker), commercial polystyrene foam (heat insulator and flotation device), and nonwoven wicks (waterway due to capillary effect). To test the effectiveness of the hydrophobic MXene membrane, a hydrophilic counterpart was also prepared. Modification of $Ti_3C_2$ with PFDTMS led to the formation of functional groups on the $-CF_3$ surface, which were responsible for the hydrophobic character. **Figure 5** shows a schematic illustration of the evaporation process of hydrophilic and hydrophobic $Ti_3C_2$ membranes. In the case of a hydrophilic membrane, the capillary effect facilitates seawater penetration, leading to the continuous crystallization of salts on the membrane surface with water evaporation. The accumulation of large amounts of salt can cause severe damage to the membrane, as shown in **Figure 5**a. However, a hydrophobic membrane is non-wettable due to its ability to block water together with dissolved salts under the membrane while vapors freely leave its pores (**Figure 5**d). Therefore, using a hydrophobic $Ti_3C_2$ membrane in a steam generator device promotes long-term and stable desalination using solar energy. For example, the concentration of the four primary ions ($Na^+$, $K^+$, $Mg^{2+}$, and $Ca^{2+}$) can be markedly reduced to the level of 99.5%, which indicates effective desalination of seawater. It was also found that the membrane was able to efficiently vaporize typical contaminants (filtration rate of about 100%) that may be contained in wastewaters, such as organic dyes, reactive dark blue (RhB) and methyl orange (MO), heavy metal ions, $Cu^{2+}$ and $Cr^{6+}$, and other organic substances, including benzene and acetone (**Figure 5**f).

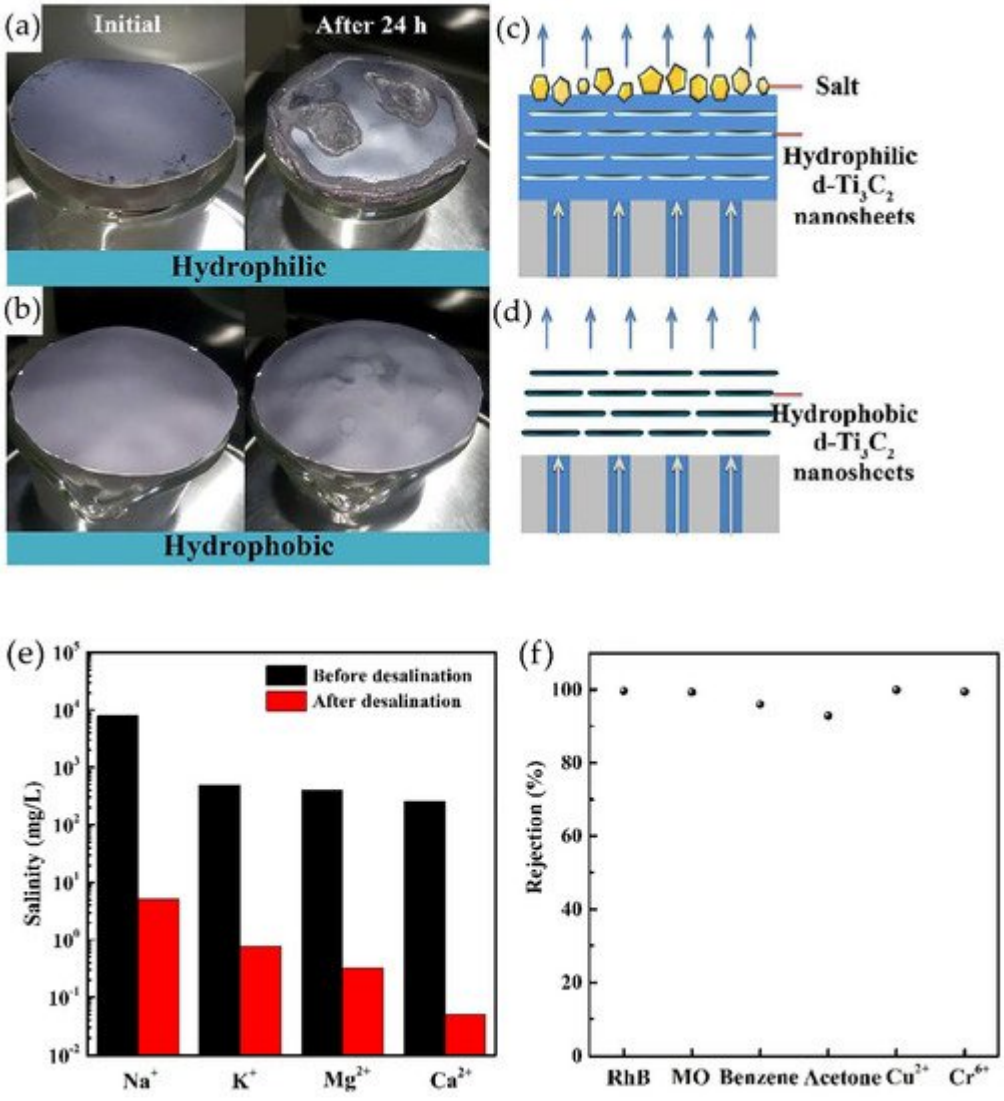

**Figure 5.** Optical photographs of (**a**) hydrophilic and (**b**) hydrophobic membranes with $Ti_3C_2$ before and after 24 h of desalination. Schematic representation of the desalination process by solar steam generation using (**c**) hydrophilic and (**d**) hydrophobic membranes. (**e**) Results of measuring the salinity of $Na^+$, $K^+$, $Mg^+$, and $Ca^+$ primary ions before and after desalination. (**f**) Filtration efficiency of organic substances and heavy metal ions. Reprinted with permission from [74] 2018 Royal Society of Chemistry.

Ju et al. [69] presented a macroporous three-dimensional MXene architecture (3DMA) for high-efficiency solar steam production. Using a two-step immersion method, such structures were obtained by applying $Ti_3C_2T_x$ MXene layers onto a melamine foam (MF) scaffold. At the first stage, the MP was immersed in polyvinyl alcohol (PVA) solution and dried in a vacuum. At the second stage, the resulting MA/PVA composite scaffold was immersed in a suspension of MXenes, followed by vacuum drying. PVA acted as an adhesion promoter between MXene and the scaffold. **Figure 6**a,b shows the difference in the morphology of melamine foam before and after modification of $Ti_3C_2T_x$. A decrease in pore size was observed as the MXene nanolayers were collected on the scaffold walls in the form of large chunks. To assess the efficiency of solar steam generation, the resulting porous structure was placed at the water–air interface while it floated freely on the water surface without any support. The efficiency of 3DMA for a solar radiation intensity of 1000 $W \cdot m^{-2}$ was 82.4% at an evaporation rate of 1.309 $kg \cdot m^{-2} \cdot h^{-1}$, and, at an illumination of 5000 $W \cdot m^{-2}$, it reached 88.1% at an evaporation rate of 6.997 $kg \cdot M^{-2} \cdot h^{-1}$ [72]. The resulting three-dimensional structure was effective for the desalination of seawater, which was manifested by a significant decrease in the concentration of $Na^+$, $K^+$, $Mg^{2+}$, and $Ca^{2+}$ cations (**Figure 6**c). In addition, when treating wastewater from methyl orange and methylene blue (MB) dyes, 3DMA demonstrated a capture rate close to 100%, as shown in **Figure 6**d.

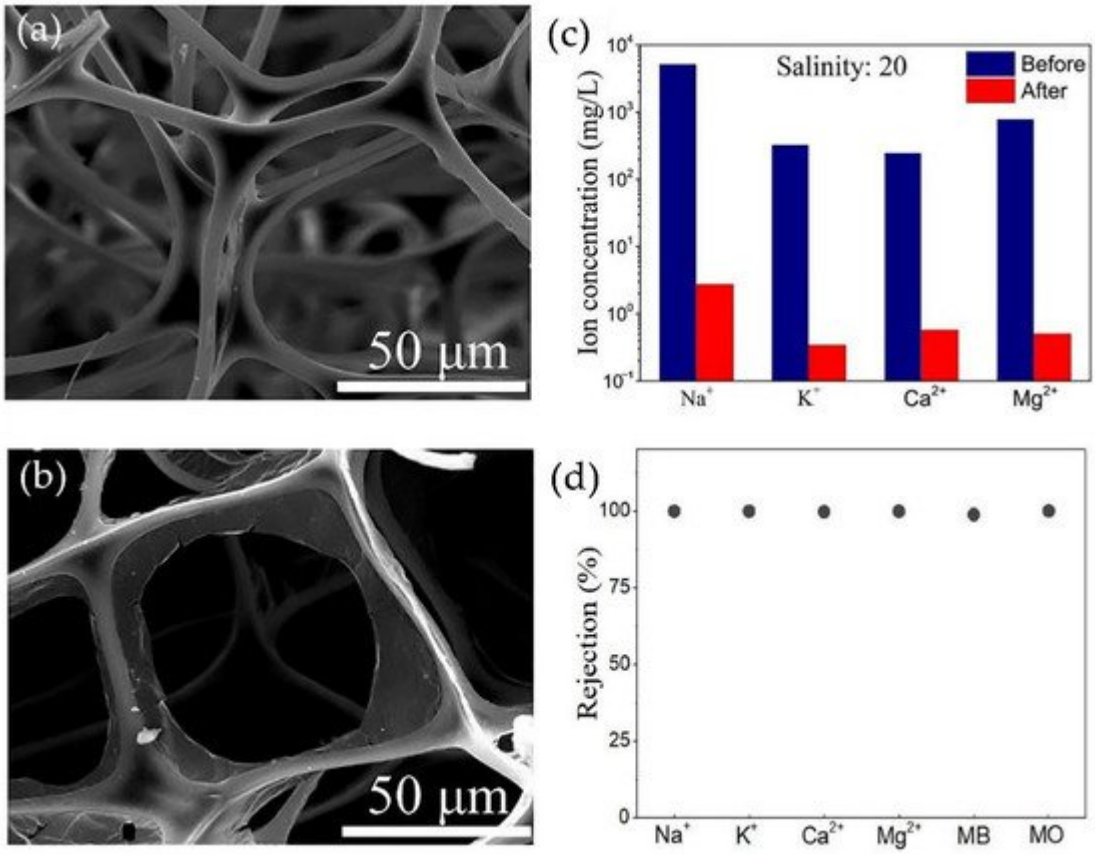

**Figure 6.** SEM images of melamine foam (**a**) before and (**b**) after immersion in a solution of polyvinyl alcohol and MXene suspension, followed by drying. (**c**) Concentrations of $Na^+$, $K^+$, $Mg^+$, and $Ca^+$ cations in a standard seawater sample with a salinity of 20 before and after evaporation. (**d**) Degree of trapping of metal ions and dyes (methylene blue, MS, and methyl orange, MO). Reprinted with permission from [72] 2019 Royal Society of Chemistry.

Additionally, a steam generator based on nanocoatings of two-dimensional $Ti_3C_2T_x$ MXene was described for the first time, which imitated the hierarchical textures of black scales of the West African gaboon viper (*Bitis rhinoceros*) [76]. MXene nanolayers were obtained by etching the $Ti_3Al_2C_2$ MAX phase in a LiF-HCl fluoride solution followed by ultrasonic-assisted delamination. The aqueous MXene solution was then sprayed onto thermosensitive polystyrene substrates and air-dried. Then, the samples were warmed up to a temperature above the glass transition temperature of polystyrene while still below 140 °C to exclude degradation of MXene. This caused them to shrink to ≈ 50% of the original length and ≈ 25% of the original area. Repeating the described deformation process several times, a biomimetic hierarchical structure of MXene was obtained, where the primary crumpled structure mimicked the micro-ridges of the black scales of vipers and the secondary structureand the secondary structure (more minor folds) resembled the texture of nano-ridges. The presence of such a branched texture of biomimetic $Ti_3C_2T_x$ nanocoatings promoted multiple scattering and reflection of light, causing broadband light absorption (84.9–86.9%) and improved equilibrium temperature at illumination of 1000 $W{\cdot}m^{-2}$ (58.2–62.6 °C) compared to conventional flat samples MXene (46.8–64.0% and 50.4–58.1 °C). An increase in the complexity of the structure (degree of deformation) of the hierarchical nanocoating caused a further increase in light absorption and thermal conductivity up to 93.2% and 65.4 °C, respectively. Solar steam generating devices based on such biomimetic MXene nanocoatings demonstrated a high evaporation rate of about 1.33 $kg{\cdot}m^{-2}{\cdot}h^{-1}$ at a solar radiation intensity of 1000 $W{\cdot}m^{-2}$. It has also been shown that they can be used to implement flexible solar/electric heaters. Consequently, the MXene surface treatment technology had a significant impact on the final performance of the device.

In 2020, Zhao et al. reported a new strategy for highly efficient solar energy conversion to steam using composite polydopamine@$Ti_3C_2T_x$ (PDA@MXene) microspheres [77]. Mixing a colloidal solution of exfoliated MXene and an aqueous dispersion of PDA led to the formation of many aggregates, which were self-assembled PDA microspheres wrapped in $Ti_3C_2T_x$ (PDA@MXene). Numerous hydrogen bonds ensured the adhesion between nanosheets and microspheres. The photothermal layer of composite microspheres demonstrated a synergistic effect in efficiently absorbing solar radiation and converting solar radiation into steam. The steam generation efficiency at an illumination of 1000 and 4000 $W{\cdot}m^{-2}$ reached 85.2% and 93.6%, respectively. In addition, the PDA@MXene photothermal layer allowed the production of pure water from seawater with a salt capture rate of over 99%. The maximum rate of water evaporation using a PDA@MXene membrane with a loading mass of microspheres of about 0.8 $mg/cm^2$ was 1.276 $kg{\cdot}m^{-2}{\cdot}h^{-1}$ at a radiation intensity of 1000 $W{\cdot}m^{-2}$. The photothermal layer of the composite was mechanically stable and effectively maintained stable light absorption and water evaporation characteristics after several lighting cycles. However, experiments with seawater desalination showed that the surface of the hydrophilic membrane becomes contaminated after 10 h of desalination due to salt

crystallization. In this case, washing off these crystals did not affect the subsequent characteristics of the evaporation of membranes based on composite PDA@MXene microspheres.

Thus, it can be concluded that MXenes, with their unique and customizable properties, provide new strategies for efficient water purification and desalination. So far, only $Ti_3C_2T_x$ was used as a photothermal material. However, strong experimental results suggest that other members of this large family of two-dimensional materials will also be effective and possibly exhibit improved light absorption and water evaporation characteristics. Therefore, MXenes show tremendous potential in generating solar power in steam to solve the problem of drinking water shortages.

### 3.2.2. Adsorption

In addition to other strategies, MXenes are actively used for another popular water purification method, namely adsorption. This is due to its simplicity, economy, and the absence of secondary pollution [78]. Adsorption is considered the most effective method for removing heavy metal ions because other strategies such as biological processing or chemical reactions cannot metabolize them or break them down. However, for the material used as an adsorbent to be effective, it has to have a large surface area and high functionality [79].

It was found that titanium exhibits a high sorption affinity for metal ions [80]. Therefore, in 2014, Peng and colleagues [42] investigated the sorption capacity of Ti-based MXene to purify water from lead ions. They suggested that, since the surface of individual $Ti_3C_2$ nanolayers possesses terminals with functional OH or F groups, the substitution of the cation in the hydroxyl group can lead to the activation of ion exchange sites, providing sites for sorption of toxic metals. Moreover, the large area of the layered MXenes promotes the binding of metal ions that have to be removed [81]. For the sorption of Pb (II), the authors proposed $Ti_3C_2(OH/ONa)_xF_{2-x}$, which was synthesized by selective etching of the $Ti_3AlC_2$ MAX phase followed by alkalinization–intercalation. As a result of the treatment, some of the terminal surface F groups were partially replaced by OH groups, and OH groups were converted to ONa groups. The results of kinetic tests showed that sorption equilibrium was reached in just 120 s. In addition, $Ti_3C_2(OH/ONa)_xF_{2-x}$ made it possible to lower the Pb (II) content in wastewater to levels below 10 µg/L. Moreover, the adsorption properties of the material were reversible. Such a high sorption capacity was associated with hydroxyl groups in activated Ti sites, where the Pb (II) ion-exchange was facilitated by forming a hexagonal potential trap. However, the residual amount of F groups weakened the adsorption of lead cations [82].

Later, papers were published in which the use of MXenes for water purification by adsorption from other toxic metals was investigated. For example, $Ti_3C_2T_x$ nanolayers synthesized by selective etching of $Ti_3AlC_2$ in a 10% HF solution followed by ultrasonic delamination have demonstrated excellent ability to remove Cr (VI) [83]. Hexavalent chromium is a strong oxidizing agent that is highly toxic to plants, animals, and humans. Improper disposal of wastewater after various industrial processes causes severe groundwater pollution and damages the environment [83]. The maximum removal capacity for Cr (VI) was 250 mg/g. At the same time, the residual concentration of hexavalent chromium after purification (less than five parts per billion) was much lower than the standard for drinking water recommended by the World Health Organization (0.05 parts per million). Removal of Cr (VI) by two-dimensional $Ti_3C_2T_x$ nanolayers occurs via a reduction reaction. MXenes reduce Cr (VI) to a less toxic form of Cr

(III), which then can be removed without alkaline treatment at an optimum pH of 5.0. It has also been shown that $Ti_3C_2T_x$ can be used for the reductive removal of other oxidants such as $K_3[Fe(CN)_6]$, $KMnO_4$, and $NaAuCl_4$.

In 2016, Wang and co-authors demonstrated for the first time the use of multilayer $V_2CT_x$ MXene as a potentially effective adsorbent for U (VI) [84]. Efficient treatment of nuclear waste is becoming a serious environmental problem, as long-lived actinide contamination threatens the environment even in small quantities due to their radiological and chemical toxicity. Therefore, the use of MXene as an adsorbent for trapping radionuclides is a promising direction. The $V_2CTx$ powder was obtained by immersing the $V_2AlC$ MAX phase powder in a 40% concentrated HF solution, followed by stirring. $V_2CT_x$ was generally stable in the process of capturing U (VI) from aqueous solution in the pH range from 3.0 to 5.0, but its sorption behavior showed a significant dependence on pH. The best results were obtained at pH 5.0. For example, the maximum absorbent capacity of a powder containing 32 at.% of the unreacted $V_2AlC$ powder was 174 mg/g. The adsorption capacity of pure two-dimensional MXene nanolayers reached about 256 mg/g. The weak binding of uranium ions at acidic pH levels (lower than 3) also suggests that multilayer $V_2CT_x$ can be regenerated with acidic solutions. Due to functional -OH/-O and -F surface groups, which play a role in the heterogeneous adsorption sites, the capture of U (VI) can be described by a heterogeneous adsorption model. The results of experiments and theoretical calculations showed that $V_2CT_x$ adsorbs uranium ions by forming bidentate adsorption configurations with hydroxyl groups attached to V atoms. The adsorption process proceeded according to the ion exchange mechanism, which was confirmed by deprotonation of the hydroxyl group after binding to U (VI).

In addition to Pb (II), Cr (VI), and U (VI), Fu et al. showed in 2020 that MXene could also adsorb Hg (II) [85]. Since mercury, which is one of the most toxic heavy metals, is widely used in the process of extraction of precious metals, e.g., from electronic devices and industrial catalysis, excessive environmental pollution causes irreparable harm to human health and natural ecosystems [86][87]. For practical use, it is desirable that the adsorbent can effectively remove Hg (II) ions from water even under harsh chemical conditions. The acid–base resistance of M-$Ti_3C_2$ nanosheets was evaluated at various pH values ranging from 1 to 12. M-$Ti_3C_2$ nanosheets (dosage 0.1 g/L) were able to remove less than 10% Hg (II) at pH ≤ 2.0. In contrast, the removal efficiency increased significantly at higher pH, and more than 99.0% of Hg (II) was removed over a wide pH range from 4 to 10. Moreover, M-$Ti_3C_2$ showed high removal efficiency (>97.0%) even in highly alkaline environments (pH > 11).

In parallel with the first experiment to remove Pb (II), it was demonstrated in 2014 that $Ti_3C_2T_x$ could also be effectively used for the adsorption of the cationic dye methylene blue (MB) [88]. The reaction of the MXene with an aqueous solution of MB under ambient conditions was described by three stages: (1) active adsorption of MB molecules on the surface of $Ti_3C_2T_x$, (2) an increase in the disordered packing of layers, and (3) oxidation of the MXene.

It has also been demonstrated that multi-layer $V_2CT_x$ MXene could be successfully used as an adsorbent for removing colorants in wastewaters. Usually, dyes in water are found in the form of ions, so they can be removed using special adsorbents. More efficient adsorption of $V_2CT_x$, compared to the most studied $Ti_3C_2T_x$ could be explained by its simpler unit cell and greater distance between the layers [89].

Due to their unique intrinsic properties, MXenes are of greater interest as adsorbents than graphene oxide, which consists of only one element and has a simpler and insufficiently functionalized surface and a high cost [82][90]. A large surface area, an abundance of active sites, and good dispersibility and reducibility, as well as the fact that many cations could spontaneously intercalate between layers of two-dimensional MXenes, make them promising candidates for water purification from toxic oxidants associated with heavy metal ions, radionuclides, and organic dyes [91]. To date, only two representatives of a large family of these materials, $Ti_3C_2T_x$ and $V_2CT_x$, have been studied as adsorbents. However, the emergence of new work with other MXenes is expected to substantially enrich the fundamental understanding of adsorption mechanisms and significantly expand the range of their possible applications for environmental cleaning.

### 3.3. Multifunctional MXene-Based Smart Textiles

The range of MXene applications is extensive, and it is hard to describe all of them in one article. Therefore, we would like to briefly mention one more interesting field where these 2D materials can be effectively implemented: wearable electronics with multifunctional characteristics. Lately, it has been shown that wearable and flexible textile-based electronics can be extremely useful due to their versatility. Such smart textile devices can be successfully applied for healthcare electronics [92], human motion monitoring [93], antibacterial [94][95], pressure sensors [96], electromagnetic interference (EMI) shielding [97], and so forth. Although multifunctional textiles are excellent candidates for wearable electronics, they have some limitations. They are connected with difficulties integrating necessary functions, such as conductivity, into the traditional textile substrates while maintaining their high intrinsic properties: breathability and flexibility [98][99]. Therefore, a search for new conductive materials that can be used for smart textiles has led to the recently discovered two-dimensional MXenes. Their unique properties allowed fabricating electronic textiles demonstrating multifunctionality.

For instance, Zhang et al. [99] reported preparing the MXene-decorated woven cotton fabrics with an interwoven conductive network. Such textile maintained the flexibility and air permeability of cotton and, in addition, gained new exciting characteristics even at the low addition of $Ti_3C_2T_x$ nanosheets. The synthesized MXene-decorated fabric showed remarkable EMI shielding, Joule heating, and strain sensing performances. The cotton textile with vertically interwoven weft and warp yarns was used. That allowed obtaining the vertically interconnected conductive networks that could increase the MXene conductivity. Meanwhile, the $Ti_3C_2T_x$ nanosheets were produced by selective etching of $Ti_3AlC_2$ MAX-phase in the HCl + LiF solution. Synthesized MXenes were then uniformly deposited onto the cotton fabric with 2−6 wt.% concentration by the spray-drying coating method. The study showed that such modified fabrics could be successfully applied as flexible heaters for warming up any bendable parts of the human body due to their outstanding Joule heating performance with a temperature up to 150 °C at an external voltage of 6 V. The MXene loading content and voltage could easily tailor the temperature of such heaters. Moreover, MXene-decorated fabric was found to be a promising candidate for the application in sensing small-range human activities since sensors on its bases exhibited high stability after 5000 cycles and superior sensitivity even at a bending strain of about 0−2.09%. MXenes with high electrical conductivity of about 48−5 Ω $sq^{-1}$ made it possible to turn simple cotton fabrics into multifunctional textiles, which can be used for wearable electronics.

Another way to employ MXene-based flexible material for electronic device-cooling applications was proposed by Liu et al. [100]. The authors produced a free-standing graphene/MXene film, demonstrating excellent thermal conductivity and heat dissipation for fire retardant ability. This composite film was produced from graphene oxide (GO), synthesized by modified Hummer's method [101], and $Ti_3C_2T_x$, prepared by selective etching of $T_{i3}AlC_2$ in HCl + LiF mixture. The vacuum-assisted filtration with a cellulose ester filter membrane was used to synthesize graphen oxide/$Ti_3C_2T_x$ film. After that, to weld the superior flexible composite graphene/MXene (GM) paper, it was reduced through immersion in hydroiodic acid, placed in a warm oil bath at 90 °C, dried at 40 °C, heated to 473 and 1000 K in an Ar atmosphere, and finally cooled down. The GM films demonstrated high thermal conductivity. At the concentration of MXene of about 40 wt.%, the thermal conductivity reached up to 26.49 W $m^{-1}$ $K^{-1}$, which was 6.71-fold and 2.93-fold higher than graphene oxide and reduced graphen oxide films. After welding graphene-MXene, more effective formation of paths for heat conduction in graphene was observed. Thus, a few reasons contributed to enhanced thermal conductivity of composites: the sp2 carbon structure of graphene and orderly alignment of MXene in the graphene matrix. Moreover, the experiment when GM paper with 40 wt.% of MXene was used as ultra-thin heat sink for LED was conducted. The results showed that a protective layer of nonconductive $TiO_2$ and graphite, appeared during combustion, provided a good flame retardant ability and outstanding heat-dissipation.

Apart from spray-drying [97][98] and vacuum-assisted filtration [102] strategies, there are also dip-coating [103] and 3D printing [104] methods. An example of the dip-coating approach is a superhydrophobic and breathable intelligent textile device with a four-core shell structure [103]. The consisting parts are the following: (1) a cheap modified elastic polypropylene textile substrate, (2) an interface polydopamine (P) layer for creating active sites for the MXene and better bonding between the MXene layer and substrate, (3) a functional MXene layer (M) of $Ti_3C_2T_x$ nanosheets, and (4) a protective polydimethylsiloxane (PDMS) layer for decreasing the MXene surface energy, preventing their oxidation, and providing a superhydrophobic ability. All the steps were performed by the dip-coating method through immersion to a certain solution regarding the layer. **Figure 7** demonstrates possible applications of a fabricated MXene-based PM/PDMS textile. This composite is expected to remarkably perform as waterproof all-in-one wearable electronics capable of tracking body motion and temperature changes due to the superior superhydrophobicity, breathability, photo-thermal and electro-thermal effects, strain and temperature sensing performance. An example of using the $Ti_3C_2T_x$ MXene/polyurethane composite fibers in the one-piece elbow sleeve, prepared by a commercial-scale flat-bed knitting machine, for tracking different movements through strain sensing and sending the signal by Bluetooth to a personal computer is presented in **Figure 7**d,e [105]. This single jersey knit of MXene/polyurethane four-ply yarn could recognize strains up to 200% and maintain stable work during 1000 stretching deformation cycles.

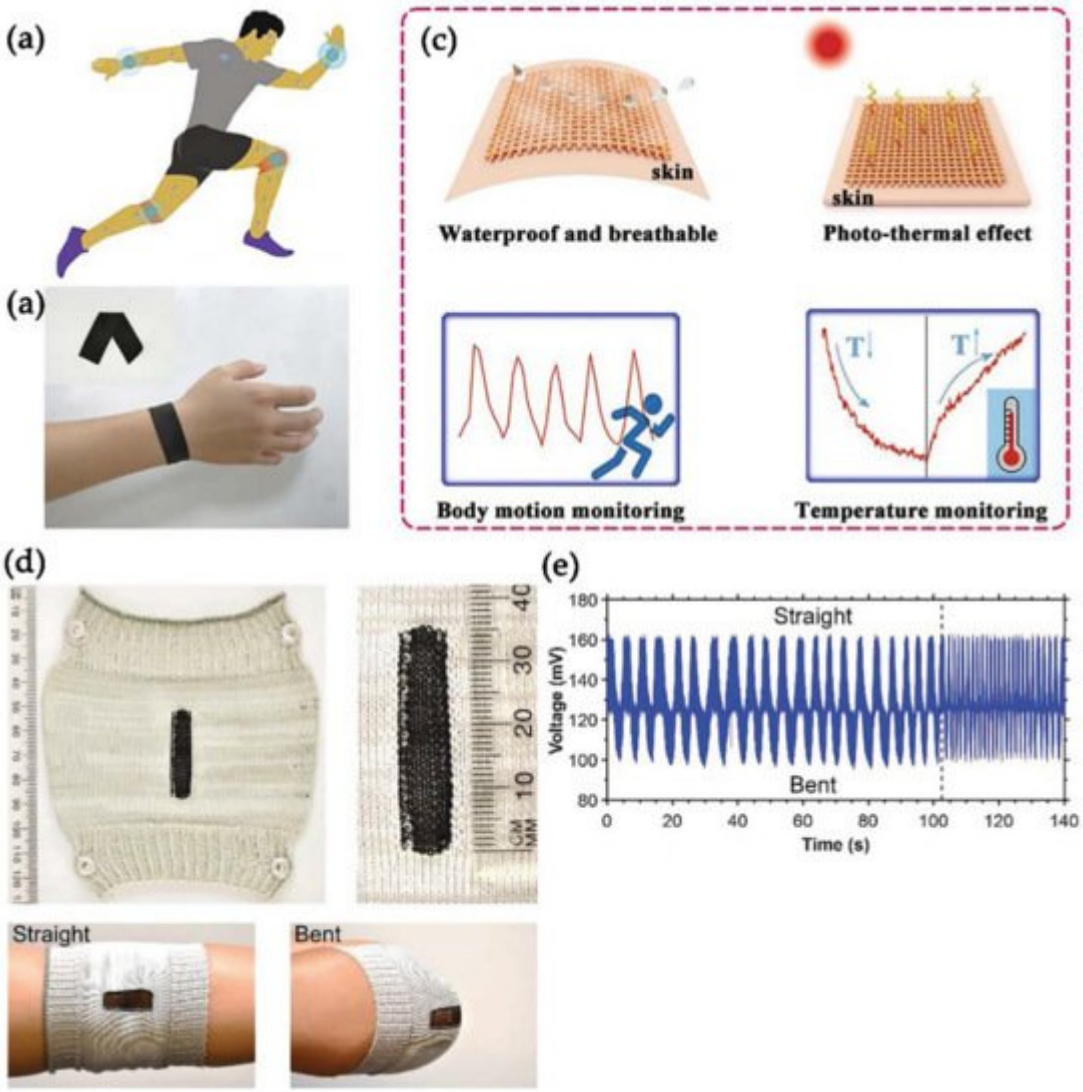


**Figure 7.** (**a**) Schematic illustration of the PM/PDMS textile attached to the joints of the human body to monitor motion actions. (**b**) A photograph of the volunteer wrist with MXene-based textile serving as a smart strain sensing device; the inset shows the photograph of one black ring textile. (**c**) Promising applications and superior properties. Reprinted with permission from [103] 2021 Elsevier. (**d**) One-piece sleeve for elbow knitted using four-ply yarn of $Ti_3C_2T_x$ MXene/polyurethane fiber in as-prepared and functioning states. (**e**) Strain sensing response of the elbow sleeve collected during continuous bending and straightening the elbow at two different frequencies (0.2 and 0.7 Hz) through a wireless Bluetooth connection. Reprinted with permission from [105] 2020 John Wiley and Sons.

3D printing can also be employed as a strategy to synthesize ideal flexible and multifunctional textiles. Cao et al. [104], for the first time, reported on the fabrication of a flexible smart textile with hybrid composite inks of TEMPO (2,2,6,6-tetramethylpiperidine-1-oxylradical)-mediated oxidized cellulose nanofibrils (TOCNFs) and $Ti_3C_2$ MXene. They prepared the $Ti_3C_2$ nanosheets from $Ti_3AlC_2$ powder by selective etching in LiF and HCl. The inks for 3D printing were obtained by mixing dispersions of TOCNFs and MXenes and magnetic stirring for 12 h at room temperature. These inks then could be transformed to continuous and stable gel TOCNFs/$Ti_3C_2$ fibers through extruding and injecting to an ethanol coagulation bath from a narrow nozzle of a 3D printer within seconds. Since these fibers possess good flexibility, they could be easily knotted after drying without causing any damage. The

TOCNFs/$Ti_3C_2$ composite fibers also demonstrated enhanced mechanical properties. That was due to the numerous functional surface groups of MXenes providing many hydrogen bonds between the $Ti_3C_2$ and TOCNFs. Thus, breaking such fibers would need a large amount of energy. The TOCNFs/$Ti_3C_2$ composite fibers and textiles showed remarkable properties through photothermal and electrothermal functions in response to multiple external photon, electron, or strain stimuli.

MXene-based textiles, apart from the above-described functions, can also provide the EMI shielding effect [106]. The electronics industry is developing rapidly as electronic devices have become an integral part of medicine, communications, computations, space, and automation. The numerous systems located close to each other cause electromagnetic interference issues [107]. EMI occurs in the radio frequency range of the electromagnetic spectrum within $10^4$–$10^{12}$ Hz [108]. Computers, fluorescent lamps, radio transmitters, and electric motors mainly radiate in the microwave range (1–40 GHz). EMI is suspected to be harmful to the human body [109][110]. Therefore, humans should be protected from the possible adverse effects of electromagnetic radiation. The way to control the influence of everyday exposure to EMI pollution is by using smart textiles capable of effective shielding [111].

EMI shielding materials first have been represented by metal-based foils, nanowires, and fibers from copper, nickel, stainless steel fiber, etc. However, the fact that such materials are heavy and susceptible to corrosion contributed to the emergence of a new class of EMI shielding materials: carbon-based composites and foams. Nevertheless, at low thickness, their protective abilities were found to be limited [112]. Therefore, the latest trend is introducing 2D MXenes into various types of fibers by different methods to achieve superior shielding characteristics [113]. The high electrical conductivity of MXenes enables the material with excellent shielding of electromagnetic waves [114].

For instance, high-elasticity and abrasion-resistant polyethylene terephthalate (PET) textiles that were dipped into$Ti_3C_2T_x$ MXene solution demonstrated superb EMI shielding properties [94]. When MXene content was about 17.2 wt.%, the modified textile showed shielding efficiency of 42.1 dB in the X-band at a small thickness of 340 µm. The primary mechanism of EMI shielding in this textile was an absorption-dominant one. This is favorable since, in such a way, the secondary EMI pollution from reflection can be significantly reduced. **Figure 8**a shows a schematic representation of the MXene-decorated textile's functioning. First, after the incident electromagnetic wave (EMW) strikes its surface, the high electrical conductivity of MXene nanosheets contributes to the reflection of a small part of the EMW. The rest EMW that entered the textile is trapped in the MXene nanosheets and is absorbed or dissipated in the form of heat within the material (textile itself has weaving and a porous structure providing an interface for effective reflection). If some part of the incident EMW is left, the multiple reflections are further absorbed and dissipated as MXene nanosheets have a large surface and interface area. The results of the electromagnetic radiation test, confirming the effectiveness of such a mechanism of EMI shielding in $Ti_3C_2T_x$/PET textile, are presented in **Figure 8**b,c. The electromagnetic radiation tester was used to record the radiation from a far-infrared radiation (FIR) therapeutic lamp and cellphone before and after covering in $Ti_3C_2T_x$/PET textile. As it can be seen, without the textile, the tester demonstrated 3703, 1378, and 433 µW $cm^{-2}$ depending on the distance from the lamp. However, after using the MXene-decorated textile, the tester showed 0 µW $cm^{-2}$ regardless of the

distance. The same behavior was observed with a cellphone that generates severe electromagnetic radiation. The EM radiation was reduced from 4989 to 0 μW $cm^{-2}$ by simply wrapping the cellphone.

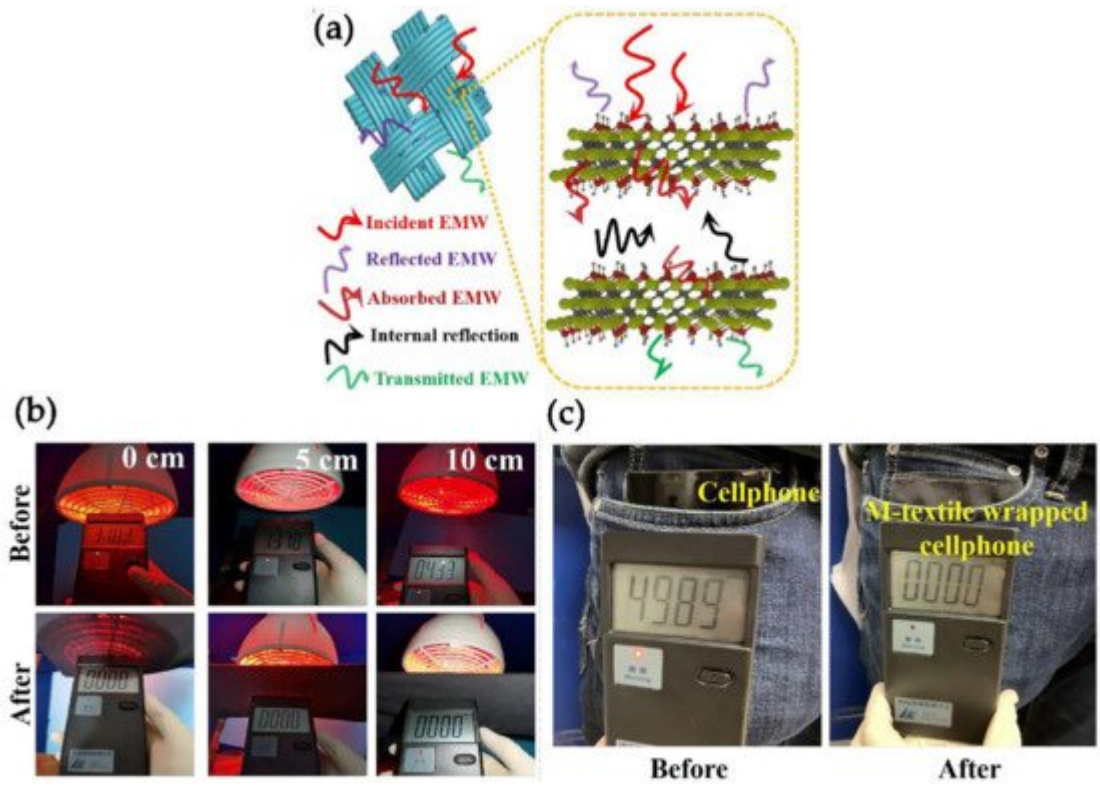


**Figure 8.** (**a**) Schematic of electromagnetic microwave dissipation in the MXene-decorated textiles. A electromagnetic radiation tester used to check the radiation before and after applying $Ti_3C_2T_x$/PET textile on a FIR lamp (**b**) and a cellphone (**c**). Reprinted with permission from [94] 2020 Royal Society of Chemistry.

The multifunctional MXene-decorated textiles are very helpful since they can be used for heating to keep warmth, protect from electromagnetic radiation generated from daily life, and sense human movements and temperature while being stretchable, breathable, and flexible. Nevertheless, assembling microscopic MXene nanosheets into macroscopic textiles can be challenging due to the irregular shape and size of the exfoliated MXenes. Many papers are devoted to $Ti_3C_2T_x$ MXene, but other members of a big family are still not discovered for smart textiles for wearable multifunctional electronics applications. The obtained results are promising, and there are plenty of effects to be explained. MXenes have remarkable mechanical properties with an ultra-high elastic modulus and excellent electrical conductivity that makes them the leading materials for smart fibers and textiles so far [115].

## References

1. Boehm, H.P.; Clauss, A.; Fischer, G.O.; Hofmann, U. Das adsorptionsverhalten sehr dunner kohlenstoff-folien. Z. Anorg. Allg. Chem. 1962, 316, 119–127.
2. Wallace, P.R. The band theory of graphite. Phys. Rev. 1947, 71, 622–634.

3. Zhen, Z.; Zhu, H. Structure and Properties of Graphene. In Graphene; Elsevier: Amsterdam, The Netherlands, 2018; pp. 1–12.
4. Xu, Z. Fundamental Properties of Praphene. In Graphene; Elsevier: Amsterdam, The Netherlands, 2018; pp. 73–102.
5. Spencer, M.J.S.; Morishita, T. (Eds.) Silicene; Springer Series in Materials Science; Springer International Publishing: Cham, Germany, 2016; Volume 235, ISBN 978-3-319-28342-5.
6. Li, X.; Zhu, H. Two-dimensional MoS2: Properties, preparation, and applications. J. Mater. 2015, 1, 33–44.
7. Akhtar, M.; Anderson, G.; Zhao, R.; Alruqi, A.; Mroczkowska, J.E.; Sumanasekera, G.; Jasinski, J.B. Recent advances in synthesis, properties, and applications of phosphorene. NPJ 2D Mater. Appl. 2017, 1, 5.
8. Bhimanapati, G.R.; Glavin, N.R.; Robinson, J.A. 2D boron nitride: Synthesis and applications. In Semiconductors and Semimetals; Elsevier: Amsterdam, The Netherlands, 2016; pp. 101–147.
9. Mashtalir, O.; Naguib, M.; Mochalin, V.N.; Dall'Agnese, Y.; Heon, M.; Barsoum, M.W.; Gogotsi, Y. Intercalation and delamination of layered carbides and carbonitrides. Nat. Commun. 2013, 4, 1716.
10. Naguib, M.; Kurtoglu, M.; Presser, V.; Lu, J.; Niu, J.; Heon, M.; Hultman, L.; Gogotsi, Y.; Barsoum, M.W. Two-dimensional nanocrystals produced by exfoliation of Ti3AlC2. Adv. Mater. 2011, 23, 4248–4253.
11. Ling, Z.; Ren, C.E.; Zhao, M.-Q.; Yang, J.; Giammarco, J.M.; Qiu, J.; Barsoum, M.W.; Gogotsi, Y. Flexible and conductive MXene films and nanocomposites with high capacitance. Proc. Natl. Acad. Sci. USA 2014, 111, 16676–16681.
12. Kim, S.; Gholamirad, F.; Yu, M.; Park, C.M.; Jang, A.; Jang, M.; Taheri-Qazvini, N.; Yoon, Y. Enhanced adsorption performance for selected pharmaceutical compounds by sonicated Ti3C2TX MXene. Chem. Eng. J. 2021, 406, 126789.
13. Naguib, M.; Mochalin, V.N.; Barsoum, M.W.; Gogotsi, Y. 25th Anniversary Article: MXenes: A new family of two-dimensional materials. Adv. Mater. 2014, 26, 992–1005.
14. Lukatskaya, M.R.; Kota, S.; Lin, Z.; Zhao, M.-Q.; Shpigel, N.; Levi, M.D.; Halim, J.; Taberna, P.-L.; Barsoum, M.W.; Simon, P.; et al. Ultra-high-rate pseudocapacitive energy storage in two-dimensional transition metal carbides. Nat. Energy 2017, 2, 17105.
15. Shahzad, F.; Alhabeb, M.; Hatter, C.B.; Anasori, B.; Man Hong, S.; Koo, C.M.; Gogotsi, Y. Electromagnetic interference shielding with 2D transition metal carbides (MXenes). Science 2016, 353, 1137–1140.

16. Naguib, M.; Mashtalir, O.; Carle, J.; Presser, V.; Lu, J.; Hultman, L.; Gogotsi, Y.; Barsoum, M.W. Two-dimensional transition metal carbides. ACS Nano 2012, 6, 1322–1331.
17. Huang, H.; Jiang, R.; Feng, Y.; Ouyang, H.; Zhou, N.; Zhang, X.; Wei, Y. Recent development and prospects of surface modification and biomedical applications of MXenes. Nanoscale 2020, 12, 1325–1338.
18. Wu, W.; Fang, H.; Ma, H.; Wu, L.; Zhang, W.; Wang, H. Boosting transport kinetics of ions and electrons simultaneously by Ti3C2Tx (MXene) addition for enhanced electrochromic performance. Nano-Micro Lett. 2021, 13, s40820.
19. Jimmy, J.; Kandasubramanian, B. Mxene functionalized polymer composites: Synthesis and applications. Eur. Polym. J. 2020, 122, 109367.
20. Xiao, Z.; Ruan, S.; Kong, L.B.; Que, W.; Zhou, K.; Liu, Y.; Zhang, T. Synthesis and Properties of MXenes. In MXenes and MXenes-Based Composites; Springer Nature Switzerland AG: Cham, Switzerland, 2020; pp. 5–93.
21. Zhang, Z.; Cai, Z.; Zhang, Y.; Peng, Y.; Wang, Z.; Xia, L.; Ma, S.; Yin, Z.; Wang, R.; Cao, Y.; et al. The recent progress of MXene-Based microwave absorption materials. Carbon N. Y. 2021, 174, 484–499.
22. Garg, R.; Agarwal, A.; Agarwal, M. A Review on MXene for energy storage application: Effect of interlayer distance. Mater. Res. Express 2020, 7, 022001.
23. Kołtunowicz, T.; Gałaszkiewicz, P.; Kierczyński, K.; Rogalski, P.; Okal, P.; Pogrebnjak, A.D.; Buranich, V.; Pogorielov, M.; Diedkova, K.; Zahorodna, V.; et al. Investigation of AC electrical properties of MXene-PCL nanocomposites for application in small and medium power generation. Energies 2021, 14, 7123.
24. Szuplewska, A.; Kulpińska, D.; Dybko, A.; Chudy, M.; Jastrzębska, A.M.; Olszyna, A.; Brzózka, Z. Future applications of MXenes in biotechnology, nanomedicine, and sensors. Trends Biotechnol. 2020, 38, 264–279.
25. Huang, K.; Li, Z.; Lin, J.; Han, G.; Huang, P. Two-dimensional transition metal carbides and nitrides (MXenes) for biomedical applications. Chem. Soc. Rev. 2018, 47, 5109–5124.
26. Li, W.; Song, Z.; Zhong, J.; Qian, J.; Tan, Z.; Wu, X.; Chu, H.; Nie, W.; Ran, X. Multilayer-structured transparent MXene/PVDF film with excellent dielectric and energy storage performance. J. Mater. Chem. C 2019, 7, 10371–10378.
27. Tu, S.; Jiang, Q.; Zhang, X.; Alshareef, H.N. Large dielectric constant enhancement in mxene percolative polymer composites. ACS Nano 2018, 12, 3369–3377.
28. Fei, M.; Lin, R.; Lu, Y.; Zhang, X.; Bian, R.; Cheng, J.; Luo, P.; Xu, C.; Cai, D. MXene-reinforced alumina ceramic composites. Ceram. Int. 2017, 43, 17206–17210.

29. Guo, J.; Legum, B.; Anasori, B.; Wang, K.; Lelyukh, P.; Gogotsi, Y.; Randall, C.A. Cold sintered ceramic nanocomposites of 2D MXene and zinc oxide. Adv. Mater. 2018, 30, 1801846.
30. Petrus, M.; Woźniak, J.; Cygan, T.; Lachowski, A.; Moszczyńska, D.; Adamczyk-Cieślak, B.; Rozmysłowska-Wojciechowska, A.; Wojciechowski, T.; Ziemkowska, W.; Jastrzębska, A.; et al. Influence of Ti3C2Tx MXene and surface-modified Ti3C2Tx MXene addition on microstructure and mechanical properties of silicon carbide composites sintered via spark plasma sintering method. Materials 2021, 14, 3558.
31. Iqbal, A.; Sambyal, P.; Kwon, J.; Han, M.; Hong, J.; Kim, S.J.; Kim, M.-K.; Gogotsi, Y.; Koo, C.M. Enhanced absorption of electromagnetic waves in Ti3C2T MXene films with segregated polymer inclusions. Compos. Sci. Technol. 2021, 213, 108878.
32. Gong, K.; Zhou, K.; Qian, X.; Shi, C.; Yu, B. MXene as emerging nanofillers for high-performance polymer composites: A review. Compos. Part B Eng. 2021, 217, 108867.
33. Wang, N.-N.; Wang, H.; Wang, Y.-Y.; Wei, Y.-H.; Si, J.-Y.; Yuen, A.C.Y.; Xie, J.-S.; Yu, B.; Zhu, S.-E.; Lu, H.-D.; et al. Robust, lightweight, hydrophobic, and fire-retarded polyimide/MXene aerogels for effective oil/water separation. ACS Appl. Mater. Interfaces 2019, 11, 40512–40523.
34. Hai, Y.; Jiang, S.; Zhou, C.; Sun, P.; Huang, Y.; Niu, S. Fire-safe unsaturated polyester resin nanocomposites based on MAX and MXene: A comparative investigation of their properties and mechanism of fire retardancy. Dalt. Trans. 2020, 49, 5803–5814.
35. Yu, B.; Yuen, A.C.Y.; Xu, X.; Zhang, Z.-C.; Yang, W.; Lu, H.; Fei, B.; Yeoh, G.H.; Song, P.; Wang, H. Engineering MXene surface with POSS for reducing fire hazards of polystyrene with enhanced thermal stability. J. Hazard. Mater. 2021, 401, 123342.
36. Kotagiri, N.; Sudlow, G.P.; Akers, W.J.; Achilefu, S. Breaking the depth dependency of phototherapy with Cerenkov radiation and low-radiance-responsive nanophotosensitizers. Nat. Nanotechnol. 2015, 10.
37. Chen, M.; Tang, S.; Guo, Z.; Wang, X.; Mo, S.; Huang, X.; Liu, G.; Zheng, N. Core-shell nanoplates as theranostic agents for in vivo photoacoustic imaging, CT imaging, and photothermal therapy. Adv. Mater. 2014, 26.
38. Yang, K.; Feng, L.; Liu, Z. Stimuli responsive drug delivery systems based on nano-graphene for cancer therapy. Adv. Drug Deliv. Rev. 2016, 105, 228–241.
39. Han, X.; Jing, X.; Yang, D.; Lin, H.; Wang, Z.; Ran, H.; Li, P.; Chen, Y. Therapeutic mesopore construction on 2D Nb2C MXenes for targeted and enhanced chemo-photothermal cancer therapy in NIR-II biowindow. Theranostics 2018, 8.
40. Yin, H.; Guan, X.; Lin, H.; Pu, Y.; Fang, Y.; Yue, W.; Zhou, B.; Wang, Q.; Chen, Y.; Xu, H. Nanomedicine-enabled photonic thermogaseous cancer therapy. Adv. Sci. 2020, 7, 1901954.

41. Lin, H.; Wang, X.; Yu, L.; Chen, Y.; Shi, J. Two-dimensional ultrathin MXene ceramic nanosheets for photothermal conversion. Nano Lett. 2017, 17, 384–391.
42. Peng, Q.; Guo, J.; Zhang, Q.; Xiang, J.; Liu, B.; Zhou, A.; Liu, R.; Tian, Y. Unique lead adsorption behavior of activated hydroxyl group in two-dimensional titanium carbide. J. Am. Chem. Soc. 2014, 136, 4113–4116.
43. Liu, G.; Zou, J.; Tang, Q.; Yang, X.; Zhang, Y.; Zhang, Q.; Huang, W.; Chen, P.; Shao, J.; Dong, X. Surface modified Ti3C2 MXene nanosheets for tumor targeting photothermal/photodynamic/chemo synergistic therapy. ACS Appl. Mater. Interfaces 2017, 9, 40077–40086.
44. Han, X.; Huang, J.; Lin, H.; Wang, Z.; Li, P.; Chen, Y. 2D ultrathin MXene-based drug-delivery nanoplatform for synergistic photothermal ablation and chemotherapy of cancer. Adv. Healthc. Mater. 2018, 7, 1701394.
45. Xing, C.; Chen, S.; Liang, X.; Liu, Q.; Qu, M.; Zou, Q.; Li, J.; Tan, H.; Liu, L.; Fan, D.; et al. Two-dimensional MXene (Ti3C2)-Integrated cellulose hydrogels: Toward smart three-dimensional network nanoplatforms exhibiting light-induced swelling and bimodal photothermal/chemotherapy anticancer activity. ACS Appl. Mater. Interfaces 2018, 10, 27631–27643.
46. Hussein, E.A.; Zagho, M.M.; Rizeq, B.R.; Younes, N.N.; Pintus, G.; Mahmoud, K.A.; Nasrallah, G.K.; Elzatahry, A.A. Plasmonic MXene-based nanocomposites exhibiting photothermal therapeutic effects with lower acute toxicity than pure MXene. Int. J. Nanomedicine 2019, 14, 4529–4539.
47. Liu, Y.; Han, Q.; Yang, W.; Gan, X.; Yang, Y.; Xie, K.; Xie, L.; Deng, Y. Two-dimensional MXene/cobalt nanowire heterojunction for controlled drug delivery and chemo-photothermal therapy. Mater. Sci. Eng. C 2020, 116, 111212.
48. Bai, L.; Yi, W.; Sun, T.; Tian, Y.; Zhang, P.; Si, J.; Hou, X.; Hou, J. Surface modification engineering of two-dimensional titanium carbide for efficient synergistic multitherapy of breast cancer. J. Mater. Chem. B 2020, 8, 6402–6417.
49. Liu, Z.; Zhao, M.; Lin, H.; Dai, C.; Ren, C.; Zhang, S.; Peng, W.; Chen, Y. 2D magnetic titanium carbide MXene for cancer theranostics. J. Mater. Chem. B 2018, 6, 3541–3548.
50. Lin, H.; Gao, S.; Dai, C.; Chen, Y.; Shi, J. A Two-dimensional biodegradable niobium carbide (MXene) for photothermal tumor eradication in NIR-I and NIR-II biowindows. J. Am. Chem. Soc. 2017, 139, 16235–16247.
51. Xiang, H.; Lin, H.; Yu, L.; Chen, Y. Hypoxia-irrelevant photonic thermodynamic cancer nanomedicine. ACS Nano 2019, 13, 2223–2235.
52. Zada, S.; Dai, W.; Kai, Z.; Lu, H.; Meng, X.; Zhang, Y.; Cheng, Y.; Yan, F.; Fu, P.; Zhang, X.; et al. Algae extraction controllable delamination of vanadium carbide nanosheets with enhanced near-

infrared photothermal performance. Angew. Chem. Int. Ed. 2020, 59, 6601–6606.

53. Rasool, K.; Helal, M.; Ali, A.; Ren, C.E.; Gogotsi, Y.; Mahmoud, K.A. Antibacterial activity of Ti3C2Tx MXene. ACS Nano 2016, 10, 3674–3684.
54. Rasool, K.; Mahmoud, K.A.; Johnson, D.J.; Helal, M.; Berdiyorov, G.R.; Gogotsi, Y. Efficient antibacterial membrane based on two-dimensional Ti3C2Tx (MXene) nanosheets. Sci. Rep. 2017, 7, 1598.
55. Mayerberger, E.A.; Street, R.M.; McDaniel, R.M.; Barsoum, M.W.; Schauer, C.L. Antibacterial properties of electrospun Ti3C2Tz (MXene)/chitosan nanofibers. RSC Adv. 2018, 8, 35386–35394.
56. Jastrzębska, A.M.; Karwowska, E.; Wojciechowski, T.; Ziemkowska, W.; Rozmysłowska, A.; Chlubny, L.; Olszyna, A. The atomic structure of Ti2C and Ti3C2 MXenes is responsible for their antibacterial activity toward E. coli bacteria. J. Mater. Eng. Perform. 2019, 28, 1272–1277.
57. Dwivedi, N.; Dhand, C.; Kumar, P.; Srivastava, A.K. Emergent 2D materials for combating infectious diseases: The potential of MXenes and MXene–graphene composites to fight against pandemics. Mater. Adv. 2021, 2, 2892–2905.
58. Arabi Shamsabadi, A.; Sharifian Gh., M.; Anasori, B.; Soroush, M. Antimicrobial mode-of-action of colloidal Ti3C2Tx MXene nanosheets. ACS Sustain. Chem. Eng. 2018, 6, 16586–16596.
59. Rozmysłowska-Wojciechowska, A.; Mitrzak, J.; Szuplewska, A.; Chudy, M.; Woźniak, J.; Petrus, M.; Wojciechowski, T.; Vasilchenko, A.S.; Jastrzębska, A.M. Engineering of 2D Ti3C2 MXene surface charge and its influence on biological properties. Materials 2020, 13, 2347.
60. Zheng, K.; Li, S.; Jing, L.; Chen, P.; Xie, J. Synergistic antimicrobial titanium carbide (MXene) conjugated with gold nanoclusters. Adv. Healthc. Mater. 2020, 9, 2001007.
61. Pandey, R.P.; Rasool, K.; Madhavan, V.E.; Aïssa, B.; Gogotsi, Y.; Mahmoud, K.A. Ultrahigh-flux and fouling-resistant membranes based on layered silver/MXene (Ti3C2Tx) nanosheets. J. Mater. Chem. A 2018, 6, 3522–3533.
62. Wu, F.; Zheng, H.; Wang, W.; Wu, Q.; Zhang, Q.; Guo, J.; Pu, B.; Shi, X.; Li, J.; Chen, X.; et al. Rapid eradication of antibiotic-resistant bacteria and biofilms by MXene and near-infrared light through photothermal ablation. Sci. China Mater. 2021, 64, 748–758.
63. Unal, M.A.; Bayrakdar, F.; Fusco, L.; Besbinar, O.; Shuck, C.E.; Yalcin, S.; Erken, M.T.; Ozkul, A.; Gurcan, C.; Panatli, O.; et al. 2D MXenes with antiviral and immunomodulatory properties: A pilot study against SARS-CoV-2. Nano Today 2021, 38, 101136.
64. Liu, X.; Wang, X.; Huang, J.; Cheng, G.; He, Y. Volumetric solar steam generation enhanced by reduced graphene oxide nanofluid. Appl. Energy 2018, 220, 302–312.

65. Xu, Y.; Yin, J.; Wang, J.; Wang, X. Design and optimization of solar steam generation system for water purification and energy utilization: A review. Rev. Adv. Mater. Sci. 2019, 58, 226–247.
66. Zhang, Y.; Wang, L.; Zhang, N.; Zhou, Z. Adsorptive environmental applications of MXene nanomaterials: A review. RSC Adv. 2018, 8, 19895–19905.
67. Li, Y.; Gao, T.; Yang, Z.; Chen, C.; Luo, W.; Song, J.; Hitz, E.; Jia, C.; Zhou, Y.; Liu, B.; et al. 3D-Printed, All-in-one evaporator for high-efficiency solar steam generation under 1 sun illumination. Adv. Mater. 2017, 29, 1700981.
68. Han, R.; Xie, Y.; Ma, X. Crosslinked P84 copolyimide/MXene mixed matrix membrane with excellent solvent resistance and permselectivity. Chinese J. Chem. Eng. 2019, 27, 877–883.
69. Ju, M.; Yang, Y.; Zhao, J.; Yin, X.; Wu, Y.; Que, W. Macroporous 3D MXene architecture for solar-driven interfacial water evaporation. J. Adv. Dielectr. 2019, 9, 1950047.
70. Pal, A.; Natu, G.; Ahmad, K.; Chattopadhyay, A. Phosphorus induced crystallinity in carbon dots for solar light assisted seawater desalination. J. Mater. Chem. A 2018, 6, 4111–4118.
71. Weinstein, L.A.; Loomis, J.; Bhatia, B.; Bierman, D.M.; Wang, E.N.; Chen, G. Concentrating solar power. Chem. Rev. 2015, 115, 12797–12838.
72. Zhao, X.; Zha, X.-J.; Pu, J.-H.; Bai, L.; Bao, R.-Y.; Liu, Z.-Y.; Yang, M.-B.; Yang, W. Macroporous three-dimensional MXene architectures for highly efficient solar steam generation. J. Mater. Chem. A 2019, 7, 10446–10455.
73. Li, R.; Zhang, L.; Shi, L.; Wang, P. MXene Ti3C2: An effective 2D light-to-heat conversion material. ACS Nano 2017, 11, 3752–3759.
74. Zhao, J.; Yang, Y.; Yang, C.; Tian, Y.; Han, Y.; Liu, J.; Yin, X.; Que, W. A hydrophobic surface enabled salt-blocking 2D Ti3C2 MXene membrane for efficient and stable solar desalination. J. Mater. Chem. A 2018, 6, 16196–16204.
75. Al-Hamadani, Y.A.J.; Jun, B.-M.; Yoon, M.; Taheri-Qazvini, N.; Snyder, S.A.; Jang, M.; Heo, J.; Yoon, Y. Applications of MXene-based membranes in water purification: A review. Chemosphere 2020, 254, 126821.
76. Li, K.; Chang, T.; Li, Z.; Yang, H.; Fu, F.; Li, T.; Ho, J.S.; Chen, P. Biomimetic MXene textures with enhanced light-to-heat conversion for solar steam generation and wearable thermal management. Adv. Energy Mater. 2019, 9, 1901687.
77. Zhao, X.; Zha, X.-J.; Tang, L.-S.; Pu, J.-H.; Ke, K.; Bao, R.-Y.; Liu, Z.; Yang, M.-B.; Yang, W. Self-assembled core-shell with synergistic solar absorption capability for highly efficient solar-to-vapor generation. Nano Res. 2020, 13, 255–264.
78. Yao, C.; Zhang, W.; Xu, L.; Cheng, M.; Su, Y.; Xue, J.; Liu, J.; Hou, S. A facile synthesis of porous MXene-based freestanding film and its spectacular electrosorption performance for organic dyes.

Sep. Purif. Technol. 2021, 263, 118365.

79. My Tran, N.; Thanh Hoai Ta, Q.; Sreedhar, A.; Noh, J.S. Ti3C2Tx MXene playing as a strong methylene blue adsorbent in wastewater. Appl. Surf. Sci. 2021, 537.
80. Choi, J.; Ide, A.; Truong, Y.B.; Kyratzis, I.L.; Caruso, R.A. High surface area mesoporous titanium–zirconium oxide nanofibrous web: A heavy metal ion adsorbent. J. Mater. Chem. A 2013, 1, 5847.
81. Kang, K.M.; Kim, D.W.; Ren, C.E.; Cho, K.M.; Kim, S.J.; Choi, J.H.; Nam, Y.T.; Gogotsi, Y.; Jung, H.-T. Selective molecular separation on Ti3C2Tx—Graphene oxide membranes during pressure-driven filtration: Comparison with graphene oxide and MXenes. ACS Appl. Mater. Interfaces 2017, 9, 44687–44694.
82. Guo, J.; Peng, Q.; Fu, H.; Zou, G.; Zhang, Q. Heavy-metal adsorption behavior of two-dimensional alkalization-intercalated MXene by First-principles calculations. J. Phys. Chem. C 2015, 119, 20923–20930.
83. Ying, Y.; Liu, Y.; Wang, X.; Mao, Y.; Cao, W.; Hu, P.; Peng, X. Two-dimensional titanium carbide for efficiently reductive removal of highly toxic chromium(VI) from water. ACS Appl. Mater. Interfaces 2015, 7, 1795–1803.
84. Wang, L.; Yuan, L.; Chen, K.; Zhang, Y.; Deng, Q.; Du, S.; Huang, Q.; Zheng, L.; Zhang, J.; Chai, Z.; et al. Loading actinides in multilayered structures for nuclear waste treatment: The first case study of uranium capture with vanadium carbide MXene. ACS Appl. Mater. Interfaces 2016, 8, 16396–16403.
85. Fu, K.; Liu, X.; Yu, D.; Luo, J.; Wang, Z.; Crittenden, J.C. Highly efficient and selective Hg(II) removal from water using multilayered Ti3C2Ox MXene via adsorption coupled with catalytic reduction mechanism. Environ. Sci. Technol. 2020, 54, 16212–16220.
86. Yang, Z.; Li, H.; Qu, W.; Zhang, M.; Feng, Y.; Zhao, J.; Yang, J.; Shih, K. Role of sulfur trioxide (SO3) in gas-phase elemental mercury immobilization by mineral sulfide. Environ. Sci. Technol. 2019, 53, 3250–3257.
87. Sun, D.T.; Peng, L.; Reeder, W.S.; Moosavi, S.M.; Tiana, D.; Britt, D.K.; Oveisi, E.; Queen, W.L. Rapid, selective heavy metal removal from water by a metal–organic framework/polydopamine composite. ACS Cent. Sci. 2018, 4, 349–356.
88. Mashtalir, O.; Cook, K.M.; Mochalin, V.N.; Crowe, M.; Barsoum, M.W.; Gogotsi, Y. Dye adsorption and decomposition on two-dimensional titanium carbide in aqueous media. J. Mater. Chem. A 2014, 2, 14334–14338.
89. Lei, H.; Hao, Z.; Chen, K.; Chen, Y.; Zhang, J.; Hu, Z.; Song, Y.; Rao, P.; Huang, Q. Insight into adsorption performance and mechanism on efficient removal of methylene blue by accordion-like V2CTx MXene. J. Phys. Chem. Lett. 2020, 11, 4253–4260.

90. Mi, X.; Huang, G.; Xie, W.; Wang, W.; Liu, Y.; Gao, J. Preparation of graphene oxide aerogel and its adsorption for Cu2+ ions. Carbon N. Y. 2012, 50, 4856–4864.
91. Kim, S.; Yu, M.; Yoon, Y. Fouling and retention mechanisms of selected cationic and anionic dyes in a Ti3C2Tx MXene-ultrafiltration hybrid system. ACS Appl. Mater. Interfaces 2020, 12, 16557–16565.
92. Lee, Y.; Park, J.; Choe, A.; Cho, S.; Kim, J.; Ko, H. Mimicking human and biological skins for multifunctional skin electronics. Adv. Funct. Mater. 2020, 30, 1904523.
93. Lou, M.; Abdalla, I.; Zhu, M.; Wei, X.; Yu, J.; Li, Z.; Ding, B. Highly wearable, breathable, and washable sensing textile for human motion and pulse monitoring. ACS Appl. Mater. Interfaces 2020, 12, 19965–19973.
94. Liu, X.; Jin, X.; Li, L.; Wang, J.; Yang, Y.; Cao, Y.; Wang, W. Air-permeable, multifunctional, dual-energy-driven MXene-decorated polymeric textile-based wearable heaters with exceptional electrothermal and photothermal conversion performance. J. Mater. Chem. A 2020, 8, 12526–12537.
95. Kyrylenko, S.; Kornienko, V.; Gogotsi, O.; Oleshko, O.; Kolesnyk, M.; Mishchenko, O.; Zahorodna, V.; Buranich, V.; Pogrebnjak, A.; Zozulia, Y.; et al. Bio-functionalization of electrospun polymeric nanofibers by Ti3C2Tx MXene. In Proceedings of the 2020 IEEE 10th International Conference Nanomaterials: Applications & Properties (NAP), Sumy, Ukraine, 9–13 November 2020; pp. 02BA10-1–02BA10-5.
96. Li, T.; Chen, L.; Yang, X.; Chen, X.; Zhang, Z.; Zhao, T.; Li, X.; Zhang, J. A flexible pressure sensor based on an MXene–textile network structure. J. Mater. Chem. C 2019, 7, 1022–1027.
97. Liu, L.; Chen, W.; Zhang, H.; Wang, Q.; Guan, F.; Yu, Z. Flexible and multifunctional silk textiles with biomimetic leaf-like MXene/silver nanowire nanostructures for electromagnetic interference shielding, humidity monitoring, and self-derived hydrophobicity. Adv. Funct. Mater. 2019, 29, 1905197.
98. Zheng, X.; Shen, J.; Hu, Q.; Nie, W.; Wang, Z.; Zou, L.; Li, C. Vapor phase polymerized conducting polymer/MXene textiles for wearable electronics. Nanoscale 2021, 13.
99. Zhang, X.; Wang, X.; Lei, Z.; Wang, L.; Tian, M.; Zhu, S.; Xiao, H.; Tang, X.; Qu, L. Flexible MXene-decorated fabric with interwoven conductive networks for integrated joule heating, electromagnetic interference shielding, and strain sensing performances. ACS Appl. Mater. Interfaces 2020, 12, 14459–14467.
100. Liu, Y.; Wu, K.; Lu, M.; Jiao, E.; Zhang, H.; Shi, J.; Lu, M. Highly thermal conductivity and flame retardant flexible graphene/MXene paper based on an optimized interface and nacre laminated structure. Compos. Part A Appl. Sci. Manuf. 2021, 141.

101. Liu, Y.; Lu, M.; Wu, K.; Yao, S.; Du, X.; Chen, G.; Zhang, Q.; Liang, L.; Lu, M. Anisotropic thermal conductivity and electromagnetic interference shielding of epoxy nanocomposites based on magnetic driving reduced graphene Compos. Sci. Technol. 2019, 174, 1–10.
102. Jia, X.; Shen, B.; Zhang, L.; Zheng, W. Waterproof MXene-decorated wood-pulp fabrics for high-efficiency electromagnetic interference shielding and Joule heating. Compos. Part B Eng. 2020, 198, 108250.
103. Luo, J.; Gao, S.; Luo, H.; Wang, L.; Huang, X.; Guo, Z.; Lai, X.; Lin, L.; Li, R.K.Y.; Gao, J. Superhydrophobic and breathable smart MXene-based textile for multifunctional wearable sensing electronics. Chem. Eng. J. 2021, 406.
104. Cao, W.; Ma, C.; Mao, D.; Zhang, J.; Ma, M.; Chen, F. MXene-reinforced cellulose nanofibril inks for 3D-printed smart fibres and textiles. Adv. Funct. Mater. 2019, 29, 1905898.
105. Seyedin, S.; Uzun, S.; Levitt, A.; Anasori, B.; Dion, G.; Gogotsi, Y.; Razal, J.M. MXene composite and coaxial fibers with high stretchability and conductivity for wearable strain sensing textiles. Adv. Funct. Mater. 2020, 30, 1910504.
106. Zhang, H.; Chen, J.; Ji, H.; Wang, N.; Feng, S.; Xiao, H. Electromagnetic interference shielding with absorption-dominant performance of Ti3C2TX MXene/non-woven laminated fabrics. Text. Res. J. 2021, 004051752110062.
107. Rubežienė, V.; Varnaitė-Žuravliova, S. EMI shielding textile materials. In Materials for Potential EMI Shielding Applications; Elsevier: Amsterdam, The Netherlands, 2020; pp. 357–378.
108. Roh, J.-S.; Chi, Y.-S.; Kang, T.J.; Nam, S. Electromagnetic shielding effectiveness of multifunctional metal composite fabrics. Text. Res. J. 2008, 78, 825–835.
109. Lee, P.-C.; Kim, B.-R.; Jeoung, S.K.; Kim, Y.K. Electromagnetic Interference Shielding Effectiveness of Polypropylene/Conducting Fiber Composites. In AIP Conference Proceedings; AIP Publishing LLC: Melville, NY, USA, 2016; p. 120015.
110. Alameri, B.M. Electromagnetic interference (EMI) produced by high voltage transmission lines. EUREKA Phys. Eng. 2020, 5, 43–50.
111. Zhou, Z.; Song, Q.; Huang, B.; Feng, S.; Lu, C. Facile fabrication of densely packed Ti3C2 MXene/nanocellulose composite films for enhancing electromagnetic interference shielding and electro-/photothermal performance. ACS Nano 2021, 15, 12405–12417.
112. Ma, C.; Cao, W.T.; Zhang, W.; Ma, M.G.; Sun, W.M.; Zhang, J.; Chen, F. Wearable, ultrathin and transparent bacterial celluloses/MXene film with Janus structure and excellent mechanical property for electromagnetic interference shielding. Chem. Eng. J. 2021, 403.
113. Wang, X.; Lei, Z.; Ma, X.; He, G.; Xu, T.; Tan, J.; Wang, L.; Zhang, X.; Qu, L.; Zhang, X. A lightweight MXene-coated nonwoven fabric with excellent flame retardancy, EMI shielding, and

electrothermal/photothermal conversion for wearable heater. Chem. Eng. J. 2021, 430, 132605.

114. Zeng, Z.; Jiang, F.; Yue, Y.; Han, D.; Lin, L.; Zhao, S.; Zhao, Y.; Pan, Z.; Li, C.; Nyström, G.; et al. Flexible and ultrathin waterproof cellular membranes based on high-conjunction metal-wrapped polymer nanofibers for electromagnetic interference shielding. Adv. Mater. 2020, 32, 1908496.

115. Wang, S.; Du, X.; Luo, Y.; Lin, S.; Zhou, M.; Du, Z.; Cheng, X.; Wang, H. Hierarchical design of waterproof, highly sensitive, and wearable sensing electronics based on MXene-reinforced durable cotton fabrics. Chem. Eng. J. 2021, 408, 127363.